Geochemical Transactions

BioMed Central

Research article

Open Access

Abiotic ammonium formation in the presence of Ni-Fe metals and alloys and its implications for the Hadean nitrogen cycle

Alexander Smirnov*[1], Douglas Hausner[2], Richard Laffers[1], Daniel R Strongin[2] and Martin AA Schoonen[1]

Address: [1]Department of Geosciences, Stony Brook University, Stony Brook, NY 11794, USA and [2]Department of Chemistry, Temple University, Philadelphia, PA 19122, USA

Email: Alexander Smirnov* - asmirnov@ms.cc.sunysb.edu; Douglas Hausner - dugh@temple.edu; Richard Laffers - rlaffers@ic.sunysb.edu; Daniel R Strongin - dstrongin@temple.edu; Martin AA Schoonen - mschoonen@notes.cc.sunysb.edu

* Corresponding author

Published: 19 May 2008

Geochemical Transactions 2008, **9**:5 doi:10.1186/1467-4866-9-5

Received: 2 October 2007
Accepted: 19 May 2008

This article is available from: http://www.geochemicaltransactions.com/content/9/1/5

Abstract

Experiments with dinitrogen-, nitrite-, nitrate-containing solutions were conducted without headspace in Ti reactors (200°C), borosilicate septum bottles (70°C) and HDPE tubes (22°C) in the presence of Fe and Ni metal, awaruite ($Ni_{80}Fe_{20}$) and tetrataenite ($Ni_{50}Fe_{50}$). In general, metals used in this investigation were more reactive than alloys toward all investigated nitrogen species. Nitrite and nitrate were converted to ammonium more rapidly than dinitrogen, and the reduction process had a strong temperature dependence. We concluded from our experimental observations that Hadean submarine hydrothermal systems could have supplied significant quantities of ammonium for reactions that are generally associated with prebiotic synthesis, especially in localized environments. Several natural meteorites (octahedrites) were found to contain up to 22 ppm N_{tot}. While the oxidation state of N in the octahedrites was not determined, XPS analysis of metals and alloys used in the study shows that N is likely present as nitride (N^{3-}). This observation may have implications toward the Hadean environment, since, terrestrial (e.g., oceanic) ammonium production may have been supplemented by reduced nitrogen delivered by metal-rich meteorites. This notion is based on the fact that nitrogen dissolves into metallic melts.

Introduction

Ammonia (NH_3) or ammonium (NH_4^+), henceforth NH_3/NH_4^+, are necessary precursors for reactions associated with prebiotic syntheses, such as the Strecker synthesis. It has been experimentally shown that NH_3/NH_4^+ environments are more efficient in organic synthesis than those dominated by dinitrogen (henceforth N_2) in both aqueous and gaseous environments [e.g., [1]] [2,3]. This notion is not unexpected, considering that, the strong triple bond (948 $kJ.mol^{-1}$) of the N_2 would presumably result in large reaction activation barriers (i.e., low conversion rates), even if the overall reaction is thermodynamically favored.

Several possible pathways to abiotic NH_3/NH_4^+ on early the Earth have been proposed: reduction of NO_2^-/NO_3^- by Fe^{++}/FeS in the ocean [e.g., [4]] [5,6]; atmospheric production from N_2 and HCN [e.g., [7]] [8]; release from rocks and minerals [e.g., [9]]; photoreduction on mineral surfaces [e.g., [10]] [11,12]; and hydrothermal aqueous reduction from N_2 in the presence of minerals under conditions typical of submarine hydrothermal systems [e.g.,

[13]] [14,15]. Each of the mechanisms relies on a different set of assumptions and none of the proposed mechanisms has, in our opinion, gained universal acceptance in the scientific community as the predominant source of abiotic NH_3/NH_4^+.

In this scientific contribution we focus on the catalytic properties of Ni and Fe metals and their alloys which can form in submarine hydrothermal systems (SHS), especially those driven by exothermic hydration reactions (e.g., serpentinization) in an off-axis tectonic setting. Upon dissolution of Ni-containing rock-forming minerals (e.g., olivine, pyroxene, amphibole), released Ni and Fe can react to form metals and alloys under extreme reducing conditions imposed on the system by the serpentinization processes [16-18]. The conditions are commonly reducing enough to stabilize Ni-Fe alloys (e.g., awaruite – Ni_3Fe), metallic nickel (Ni^0) and even iron (Fe^0). These minerals occur regularly, albeit in small quantities in both ancient and modern serpentinites [19-26]. A compilation of representative chemical analyses of metals and alloys found in serpentinites is presented in Fig. 1. The observations from natural systems have been corroborated by laboratory experiments [27,28].

An active global tectonic cycle is not required for the formation and operation of serpentinization-driven SHS and hence we assume that these environments were commonly present on the Hadean Earth. Moreover, the lack of oxygen and the possible presence of significant amounts of hydrogen gas in the Hadean atmosphere (and consequently in the ocean water) may have further enhanced the stability of base metals and their alloys [29,30].

The most abundant reactant for abiotic NH_3/NH_4+ formation in the Hadean was N_2 dissolved in the seawater from the N_2-rich atmosphere. NO_2^- and NO_3^- are also thought to have been available, although likely in low concentrations. These oxidized N species could have formed in high energy events such as lightning, corona discharge and/or impacts and subsequently rain out into the ocean [31-34].

In this contribution we report the results of an experimental study undertaken to evaluate the hypothesis that abiotic NH_4^+ formation from dissolved N_2, NO_2^- and NO_3^- in the presence of Ni_3Fe, NiFe, Ni^0 and Fe^0 was an operative synthetic route at anaerobic conditions potentially present in the Hadean Ocean. Furthermore, we attempt to quantify global NH_4^+ yields in the Hadean Ocean produced by investigated mechanisms.

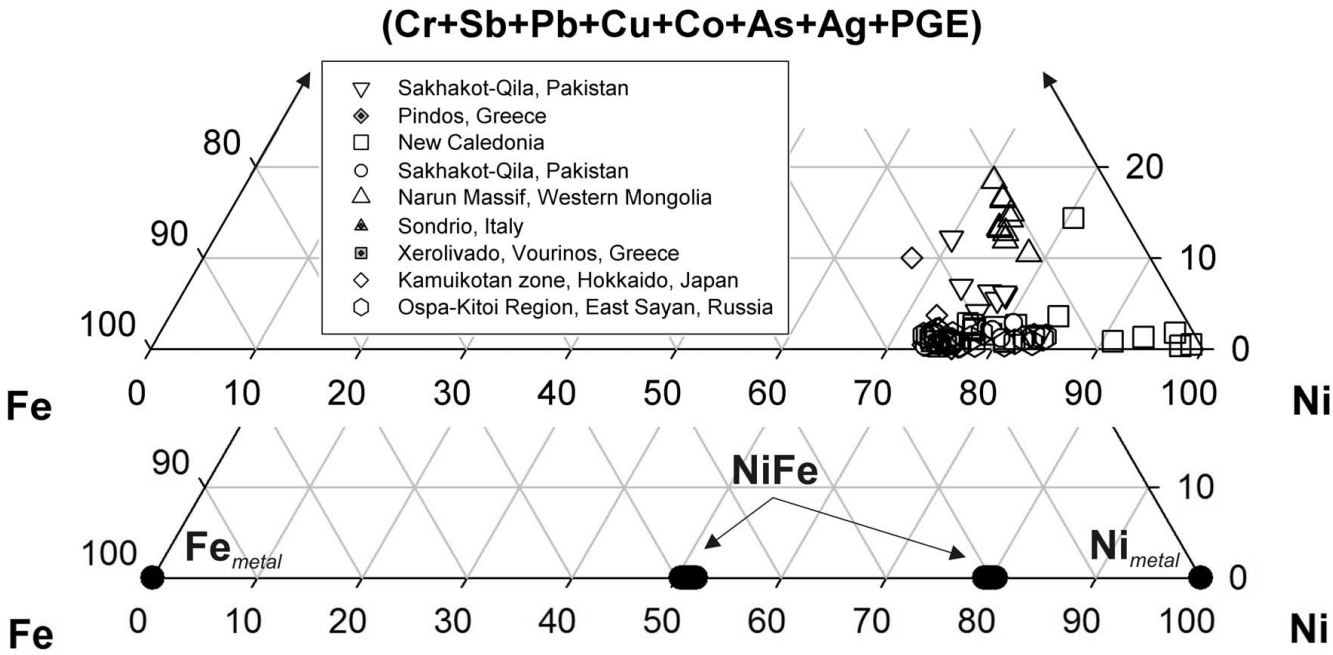

Figure 1
A ternary diagram of naturally occurring Ni-Fe-M (M = Cr, Sb, Pb, Cu, Co, As, Ag, PGE) alloys and their comparison to synthetic alloys used in this study. Analyses of natural samples were adapted from: [19] [22] [109-115]. Each data point represents an electron microprobe analysis expressed in weight percent.

Methods and materials

Reduction experiments

Three sets of experiments were conducted at three different temperatures: 200°C (runs 1–36), 70°C (runs 37–59) and 22°C (runs 60–83). The choice of reactors was based on experimental temperature: 15 mL passivated HIP® Titanium 64 tube reactors (200°C); 20 mL I-Chem® borosilicate vials with PTFE/Si septum caps (70°C) and 15 mL BD HDPE Falcon® tubes (22°C). Reactors were kept at constant temperature in a heated water bath (20, 70°C) or an Isotemp® oven (200°C). All experiments lasted 24 hours and were conducted in the absence of headspace (e.g., no gas phase). No additional pressure other than that of expanding liquid was imposed on the vessels (~400 psi/27 bars with Ni^0 to ~800 psi/55 bars with Fe^0 at 200°C).

All reacting solutions were prepared from freshly drawn UV/UF deionized water (henceforth DI) either by purging with a UHP gas of interest (e.g., Ar, N_2, H_2/N_2) and/or by dissolving appropriate amounts of reagents. NH_4^+ content of all unreacted reagent solutions (e.g., blanks) was below the detection limit of ion chromatography (<0.1 μmol.kg^{-1}, reported by the manufacturer). DI purged with N_2 gas under ambient conditions results in equilibrium N_2(aq) concentration of 0.59 mmol.kg^{-1}. The effect of O_2 was, however, also determined (runs 39, 41, 45, 47, 50, 52, 56, 58, 62, 64, 68, 70, 74, 76, 80, 82) in experiments with DI equilibrated with present-day atmosphere (e.g., no N_2 purging).

To ensure clean and fresh mineral surfaces (e.g., free of oxidation products and/or atmospheric sorbed gases), all metal/alloys were ultrasonically cleaned for 1 hour in 0.06 M HCl immediately preceding the experiments. Subsequently they were washed three times with the designated reacting solution and loaded into reactors in the form of slurry. This "wet loading" procedure eliminated sorption of gases from the atmosphere onto freshly cleaned metal surfaces which was especially important in blank experiments.

Background NH_4^+ production (e.g., release from reactants, reaction vessels, etc.) was assessed in blank experiments with Ar-saturated solutions and no added N source (runs 1, 9, 17, 25, 37, 43, 49, 54, 60, 66, 72, 78). NO_3^- and NO_2^- solutions were prepared by dissolution of ACS reagent grade KNO_3 and KNO_2, respectively. The pH was not buffered and was allowed to change as a result of solution-metal/alloy interactions and was recorded before and after the experiment. After pH measurements, all samples were acidified with 0.2 M HCl to ensure the conversion of NH_3 to NH_4^+ and to prevent the formation of Fe precipitates. The samples were stored at 1°C and analyzed within 24 – 48 hours. The summary of all experimental conditions is presented in Tab. 1.

Analysis of solids, their surfaces, and reaction products

Metals and alloys representing an fcc solid solution of Ni in Fe were purchased from Alfa Aesar® and Goodfellow. All starting and selected reacted solids were characterized by X-Ray Diffractometry, X-Ray Photoelectron Spectroscopy, Scanning Electron Microscopy, B.E.T. surface analysis, and Electron Microprobe. The results of metal/alloy characterization are summarized in Tab. 2 and Fig. 2, 3.

X-Ray Diffraction (XRD) data were collected using a Scintag PAD X diffractometer under the following conditions: CuKα1, 40 kV, 25 mA, 5° – 90° 2Θ, step 0.02° 2Θ and variable scan rates.

Scanning Electron Analysis (SEM) was performed on the LEO 1550 SFEG scanning electron microscope equipped with an EDAX energy dispersive X-ray spectrometer (EDS) using an accelerating voltage of 15 kV and a 30 μm aperture.

Oxidation state of Ni, Fe and the presence of N in alloys were determined by X-Ray Photoelectron Spectroscopy (XPS). The data were acquired with unmonochromatized $Mg_{K\alpha}$ and $Al_{K\alpha}$ radiation at 1253.6 eV and 1486.7 eV using a Physical Electronics source controller in a vacuum chamber with a base pressure of 1×10^{-9} Torr. A VG Microtech hemispherical analyzer was used to obtain the energy distribution of the photoemitted electrons at pass energies of 50 and 75 eV. The binding energies were calibrated by fixing the Au 4p3/2 and 4f7/2 peaks (546.3 eV, 87.5 eV) from a gold standard, and the metallic Fe 2p3/2 and Ni 2p3/2 cores (707.0 eV, 852.3 eV). Selected particles were sputtered with Ar^+ accelerated to 2 kV to expose their inte-

Table 1: Physical and chemical characteristics of alloys/metals used in study. Formula and the "*a*" parameter determined from EPMA analyses and from LeBail refinement of XRD data, respectively. The chemical composition of Ni-Fe alloys was confirmed by EPMA as: $Ni_{49.78(\pm 0.49)}Fe_{50.22(\pm 0.49)}$ and $Ni_{79.14(\pm 0.43)}Fe_{20.86(\pm 0.43)}$.

Metal/Alloy	*Formula*	*Manufacturer*	*Surface Area [m²]*	*Space Group*	*Unit cell [Å]*	*Natural analog*
Iron	Fe	Alfa Aesar	0.6536 ± 0.0776	Im-3m	2.866(1)	Iron
Nickel	Ni	Alfa Aesar	0.5044 ± 0.0309	Fm-3m	3.523(1)	Nickel
$Ni_{50}Fe_{50}$	NiFe	Goodfellow	0.3685 ± 0.0094	Fm-3m	3.586(3)	Tetrataenite
$Ni_{81}Fe_{19}$	$Ni_{3.7}Fe$	Goodfellow	0.1877 ± 0.0131	Fm-3m	3.547(6)	Awaruite

Table 2: Conditions and results of reduction experiments conducted in this study. All concentrations are in μmol.kg^{-1}. Values and their errors bigger than 10 are rounded to the nearest whole number, those smaller than 10 are rounded to the nearest tenth.

Metal/Alloy	*Run*	*Solution*	*T°C*	pH_{pre}	pH_{post}	NH_4^+	%	$NH_4^+{}_{norm}$*	NO_2^-**	NO_3^-**
Fe	1	Ar	200	5.7	9.9	171 ± 1	-	340 ± 21	n.a.	n.a.
Fe	2	650 N_2	200	5.8	8.9	187 ± 1	2.5	371 ± 23	n.a.	n.a.
Fe	3	39/617 H_2/N_2	200	5.8	8.4	230 ± 1	10	455 ± 28	n.a.	n.a.
Fe	4	459 KCl in N_2	200	6.2	8.9	267 ± 2	15	529 ± 32	n.a.	n.a.
Fe	5	484 KNO_2 in N_2	200	6.0	9.8	768 ± 1	100	1522 ± 93	0	0
Fe	6	465 KNO_3 in N_2	200	6.2	9.8	760 ± 8	100	1507 ± 92	0	0
Fe	7	485 KNO_2 in Ar	200	6.0	10.2	749	100	1486 ± 91	0	0
Fe	8	477 KNO_3 in Ar	200	6.2	10.3	752 ± 3	100	1491 ± 91	0	0
Ni	9	Ar	200	5.8	8.7	18	-	27 ± 3	n.a.	n.a.
Ni	10	650 N_2	200	5.7	8.3	28	1.5	43 ± 5	n.a.	n.a.
Ni	11	39/617 H_2/N_2	200	5.8	6.3	30	1.8	45 ± 5	n.a.	n.a.
Ni	12	459 KCl in N_2	200	6.2	6.7	20	0.3	30 ± 4	n.a.	n.a.
Ni	13	484 KNO_2 in N_2	200	6.0	9.1	559 ± 8	100	855 ± 102	0	0
Ni	14	465 KNO_3 in N_2	200	6.2	9.0	538 ± 7	100	823 ± 98	0	0
Ni	15	485 KNO_2 in Ar	200	6.0	9.3	544 ± 7	100	833 ± 99	0	0
Ni	16	477 KNO_3 in Ar	200	6.2	9.3	543 ± 4	100	830 ± 99	0	0
$Ni_{50}Fe_{50}$	17	Ar	200	5.8	8.7	15	-	40 ± 1	n.a.	n.a.
$Ni_{50}Fe_{50}$	18	650 N_2	200	5.7	7.9	17	0.3	47 ± 1	n.a.	n.a.
$Ni_{50}Fe_{50}$	19	39/617 H_2/N_2	200	5.6	8	17	0.3	45 ± 1	n.a.	n.a.
$Ni_{50}Fe_{50}$	20	476 KCl in N_2	200	6.3	7.1	14	0	39 ± 1	n.a.	n.a.
$Ni_{50}Fe_{50}$	21	480 KNO_2 in N_2	200	5.9	9.8	418 ± 3	100	1133 ± 29	0	0
$Ni_{50}Fe_{50}$	22	463 KNO_3 in N_2	200	6.0	9.7	490 ± 2	100	1330 ± 34	0	0
$Ni_{50}Fe_{50}$	23	474 KNO_2 in Ar	200	6.1	10.3	475 ± 5	100	1289 ± 33	0	0
$Ni_{50}Fe_{50}$	24	487 KNO_3 in Ar	200	6.0	9.9	476 ± 6	100	1293 ± 33	0	0
$Ni_{81}Fe_{19}$	25	Ar	200	5.8	8.6	18	-	98 ± 7	n.a.	n.a.
$Ni_{81}Fe_{19}$	26	650 N_2	200	5.7	7.9	19	0.2	99 ± 7	n.a.	n.a.
$Ni_{81}Fe_{19}$	27	39/617 H_2/N_2	200	5.6	8.3	19	0.2	103 ± 7	n.a.	n.a.
$Ni_{81}Fe_{19}$	28	476 KCl in N_2	200	6.3	6.2	18 ± 1	0	96 ± 7	n.a.	n.a.
$Ni_{81}Fe_{19}$	29	480 KNO_2 in N_2	200	5.9	9.9	410 ± 6	100	2186 ± 153	0	0
$Ni_{81}Fe_{19}$	30	463 KNO_3 in N_2	200	6.0	9.8	483 ± 4	100	2576 ± 180	0	0
$Ni_{81}Fe_{19}$	31	474 KNO_2 in Ar	200	6.1	10.3	485 ± 4	100	2583 ± 180	0	0
$Ni_{81}Fe_{19}$	32	487 KNO_3 in Ar	200	6.0	9.9	493 ± 3	100	2626 ± 183	0	0
-	33	497 KNO_2	200	6.0	9.4	45	9.1	-	288 ± 2	73 ± 1
-	34	444 KNO_3	200	6.1	6.4	3.6	0.8	-	273 ± 1	129 ± 1
-	35	506 $FeCl_2$ in N_2	200	4.7	3.3	8.1 ± 0.1	1.2	-	n.a.	n.a.
-	36	492 $NiCl_2$ in N_2	200	5.3	5.7	8.0 ± 0.3	1.2	-	n.a.	n.a.
Fe	37	Ar	70	5.7	7.6	3.8	-	7.4 ± 0.5	n.a.	n.a.
Fe	38	650 N_2	70	5.8	8.5	3.6	0	7.2 ± 0.4	n.a.	n.a.
Fe	39	492 KNO_2 in O_2	70	6.9	10.1	559 ± 3	100	1107 ± 68	0	0
Fe	40	502 KNO_2 in N_2	70	6.1	9.8	550 ± 3	100	1091 ± 67	0	0
Fe	41	511 KNO_3 in O_2	70	6.7	9.9	558 ± 2	98	1106 ± 68	0	8.8 ± 0.2
Fe	42	486 KNO_3 in N_2	70	6.3	10.1	512 ± 6	98	1015 ± 62	0	9.6 ± 0.2
Ni	43	Ar	70	5.7	7.6	0.9	-	1.4 ± 0.2	n.a.	n.a.
Ni	44	650 N_2	70	5.8	6.9	0.9	0	1.4 ± 0.2	n.a.	n.a.
Ni	45	492 KNO_2 in O_2	70	6.9	10.1	528 ± 2	100	807 ± 96	0	0
Ni	46	502 KNO_2 in N_2	70	6.1	9.9	534 ± 3	100	818 ± 97	0	0
Ni	47	511 KNO_3 in O_2	70	6.7	10.2	521 ± 5	100	797 ± 95	0	0
Ni	48	486 KNO_3 in N_2	70	6.3	10.2	534 ± 5	100	817 ± 97	0	0
$Ni_{50}Fe_{50}$	49	Ar	70	5.7	8.2	0.4	-	1.2	n.a.	n.a.
$Ni_{50}Fe_{50}$	50	650 N_2	70	5.8	8.3	0.4	0	1.2	n.a.	n.a.
$Ni_{50}Fe_{50}$	50	492 KNO_2 in O_2	70	6.9	8.4	22 ± 1	3.9	61 ± 2	473 ± 3	0
$Ni_{50}Fe_{50}$	51	502 KNO_2 in N_2	70	6.1	8.1	23 ± 1	2.8	62 ± 2	488 ± 2	0
$Ni_{50}Fe_{50}$	52	511 KNO_3 in O_2	70	6.7	8.0	19 ± 1	8	53 ± 1	0	470 ± 2
$Ni_{50}Fe_{50}$	53	486 KNO_3 in N_2	70	6.3	8.4	28 ± 1	6.2	77 ± 2	0	456 ± 2
$Ni_{81}Fe_{19}$	54	Ar	70	5.7	8.2	0.5	-	2.9 ± 0.2	n.a.	n.a.
$Ni_{81}Fe_{19}$	55	650 N_2	70	5.8	8.1	0.5	0	2.7 ± 0.2	n.a.	n.a.
$Ni_{81}Fe_{19}$	56	492 KNO_2 in O_2	70	6.9	9.2	23 ± 1	4.7	125 ± 9	410 ± 1	0
$Ni_{81}Fe_{19}$	57	502 KNO_2 in N_2	70	6.1	9.2	71 ± 2	14	379.27	406 ± 1	0

Table 2: Conditions and results of reduction experiments conducted in this study. All concentrations are in μmol.kg^{-1}. Values and their errors bigger than 10 are rounded to the nearest whole number, those smaller than 10 are rounded to the nearest tenth. *(Continued)*

$Ni_{81}Fe_{19}$	58	511 KNO_3 in O_2	70	6.7	8.6	35	6.8	186 ± 13	13 ± 1	425 ± 2
$Ni_{81}Fe_{19}$	59	486 KNO_3 in N_2	70	6.3	8.7	69 ± 2	14.2	370 ± 26	9.1 ± 0.7	424 ± 3
Fe	60	Ar	22	5.7	6.4	0.7	-	1.4	n.a.	n.a.
Fe	61	650 N_2	22	5.8	6.6	0.7	0	1.4	n.a.	n.a.
Fe	62	541KNO_2 in O_2	22	6.2	10.8	544 ± 6	100	1078 ± 66	0	0
Fe	63	549 KNO_2 in N_2	22	6.0	10.6	542 ± 5	99	1075 ± 66	0	0
Fe	64	529 KNO_3 in O_2	22	6.4	10.5	527 ± 4	100	1044 ± 64	0	0
Fe	65	521 KNO_3 in N_2	22	5.9	10.8	486 ± 5	93	963 ± 59	0	0
Ni	66	Ar	22	5.7	6.9	0.4	-	0.6	n.a.	n.a.
Ni	67	650 N_2	22	5.8	5.6	0.4	0	0.6	n.a.	n.a.
Ni	68	541KNO_2 in O_2	22	6.2	10.6	422 ± 3	78	646 ± 77	0	0
Ni	69	549 KNO_2 in N_2	22	6.0	10.7	451 ± 5	82	690 ± 82	0	0
Ni	70	529 KNO_3 in O_2	22	6.4	10.2	139	26	213 ± 25	43	36
Ni	71	521 KNO_3 in N_2	22	5.9	10.1	364 ± 1	70	557 ± 66	1.2	22
$Ni_{50}Fe_{50}$	72	Ar	22	5.7	6.3	0	-	0	n.a.	n.a.
$Ni_{50}Fe_{50}$	73	650 N_2	22	5.8	6.3	0	0	0	n.a.	n.a.
$Ni_{50}Fe_{50}$	74	541 KNO_2 in O_2	22	6.2	6.8	1.4	0.3	3.9 ± 0.1	553 ± 2	0
$Ni_{50}Fe_{50}$	75	549 KNO_2 in N_2	22	6.0	7.7	1.1 ± 0.1	0.2	3.1 ± 0.1	556	0
$Ni_{50}Fe_{50}$	76	529 KNO_3 in O_2	22	6.4	7.2	0.8	0.2	2.1 ± 0.1	0	526 ± 1
$Ni_{50}Fe_{50}$	77	521 KNO_3 in N_2	22	5.9	7.3	1	0.2	2.7 ± 0.1	0	523 ± 2
$Ni_{81}Fe_{19}$	78	Ar	22	5.7	6.9	0	-	0	n.a.	n.a.
$Ni_{81}Fe_{19}$	79	650 N_2	22	5.8	6.6	0	0	0	n.a.	n.a.
$Ni_{81}Fe_{19}$	80	541 KNO_2 in O_2	22	6.2	9.4	3 ± 0.1	0.6	16 ± 1	515 ± 2	0
$Ni_{81}Fe_{19}$	81	549 KNO_2 in N_2	22	6.0	9.3	1.9 ± 0.1	0.4	10 ± 1	539 ± 3	0
$Ni_{81}Fe_{19}$	82	529 KNO_3 in O_2	22	6.4	8.9	0	0	0	0	493 ± 1
$Ni_{81}Fe_{19}$	83	521 KNO_3 in N_2	22	5.9	9.0	1.9 ± 0.1	0.4	10 ± 1	0	482

"n.a." denotes "not analyzed, "-" not applicable. * denotes NH_4^+ concentration formed in the experiment normalized to 1 m^2 of surface area of the metal/alloy. ** denote residual concentration after the experiment was completed.

rior and check for the presence of nitrogen using a Physical Electronics ion gun controller.

B.E.T. surface analysis (BET) was performed using a Micromeritics ASAP 2010 analyzer with a 10-mm Hg transducer using UHP N_2 gas. The surface area was calculated from measurements at 5 different N_2(g) pressures (42.58196, 85.30770, 132.82384, 180.25029 and 227.66101 Torr).

Chemical composition of alloys/metals was determined by a Cameca Camebax Micro electron microprobe (EPMA) equipped with four wavelength dispersive spectrometers and a Kevex Analyst 8000 energy dispersive detector. During all analyses, the accelerating voltage and beam current used were 15 kV and 10 nA (nominal), respectively.

Molecular hydrogen was analyzed on a SRI 8610C single column gas chromatograph (GC) with a TCD detector, 6' Hayesep D column and N_2 carrier gas. The sample (~0.2 mL) was withdrawn from the reaction vessel into a gastight® Hamilton™ syringe with a Mininert™ valve and immediately analyzed using a 4-point calibration curve. Gas mixtures (Matheson™) of known composition were used as calibration standards.

Total nitrogen content of metals/alloys was analyzed by IMR Test Labs (Lansing, NY) by inert gas fusion [35]. During the analysis, N is released from the metal at 1900°C into the stream of He gas and analyzed in a thermal conductivity cell.

Experimental solutions were analyzed for NH_4^+ using a Dionex DX-500 ion chromatograph (IC) with a 100 μL sample loop. NH_4^+ and NO_3^-/NO_2^- were analyzed using a 4 mm Dionex IonPac® CS-16 (40°C, 34 mN H_2SO_4 eluent) and IonPac® AS4A-SC (22°C, 5 mmol.kg^{-1} $Na_2B_4O_7$ eluent), respectively. Concentrations were calculated from a 4-point calibration curve with R^2 values above 0.99.

No other compounds were analyzed. It is expected, however, that other reaction products and/or intermediates (e.g., NO) may have formed during a complex sequence of electron transfer reactions.

Geochemical equilibrium modeling was performed with the Geochemist's Workbench 5 [36] software package with the thermo.com.V8.R6.full thermodynamic database complemented with data for Ni_3Fe and NiFe [37].

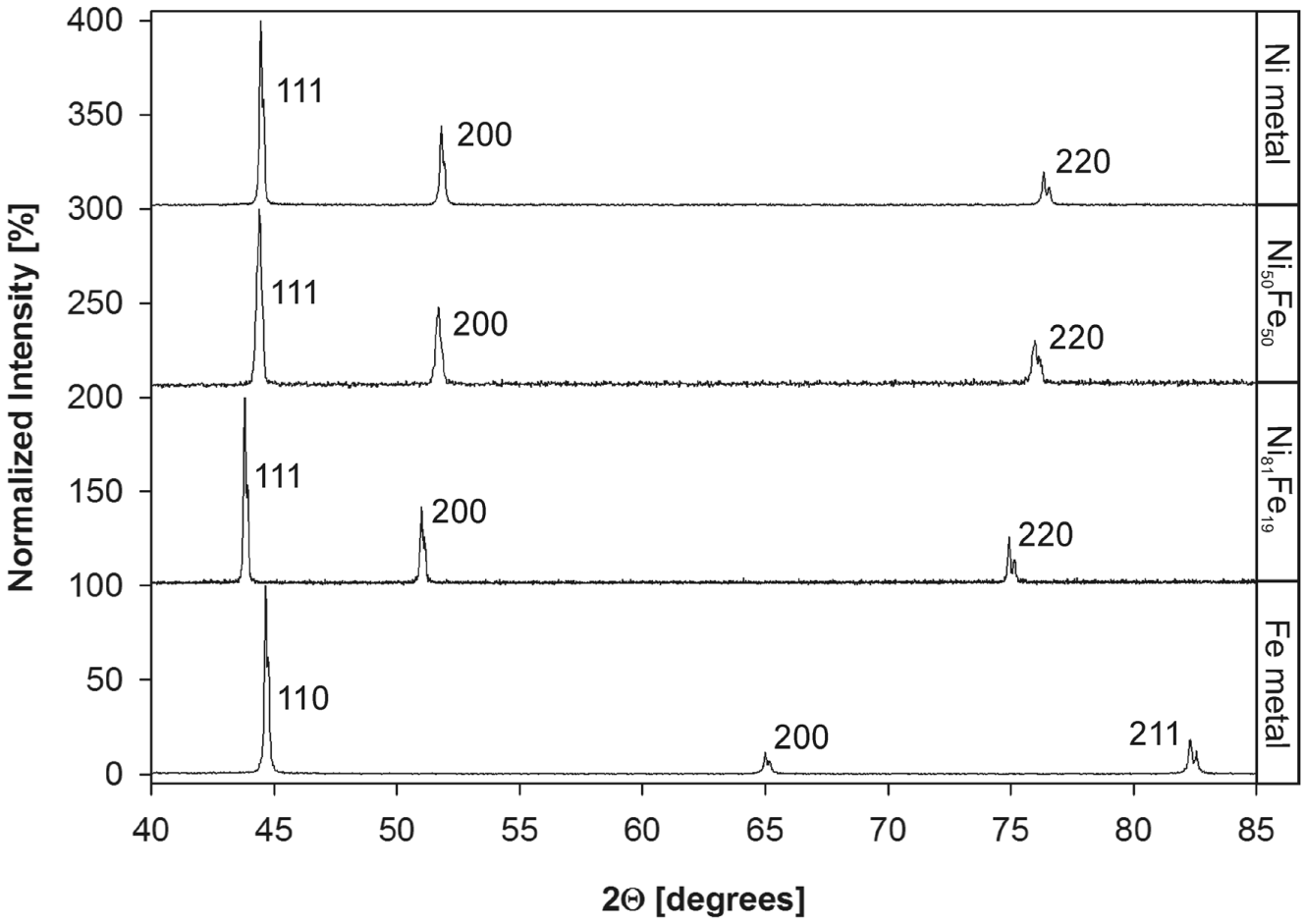

Figure 2
XRD patterns of metals/alloys used in this study. Note the similarity in patterns of Ni, $Ni_{50}Fe_{50}$ and $Ni_{81}Fe_{19}$ stemming from the same space group (Fm-3m). Fe^0 possesses Im-3m space group.

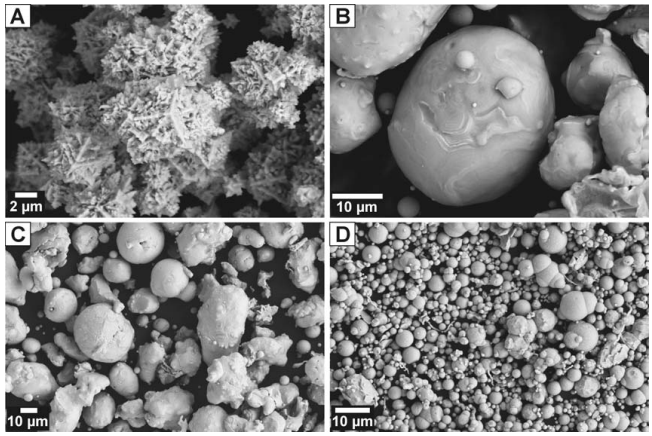

Figure 3
SEM photographs of unreacted alloys/metals used in this study. A) Ni metal, b) $Ni_{81}Fe_{19}$, c) $Ni_{50}Fe_{50}$ and d) Fe metal.

Results

Dinitrogen reduction

The results of NH_4^+ formation from N_2 and the effect of added H_2 and KCl at 200°C (normalized to 1 m^2 surface area) are shown in Fig. 4 and summarized in Tab. 1 (runs 1–32). All results are compared with respect to blank experiments conducted with Ar and no N_2 added. The blank experiments thus represent the background NH_4^+ production from the metal/alloy involved and reactor catalysis. Error bars were calculated by propagating errors from solution dilutions and B.E.T. and IC analyses. Due to relatively large error bars, only results differing from the blank (or each other) by more than the calculated error will be discussed.

In the presence of N_2, only $Ni_{81}Fe_{19}$ did not show appreciable activity toward NH_4^+ formation (Fig. 4d). Within our experimental certainty, Fe^0 was the material associated with the most NH_4^+ production (31 $\mu mol.kg^{-1}.m^2$, Fig.

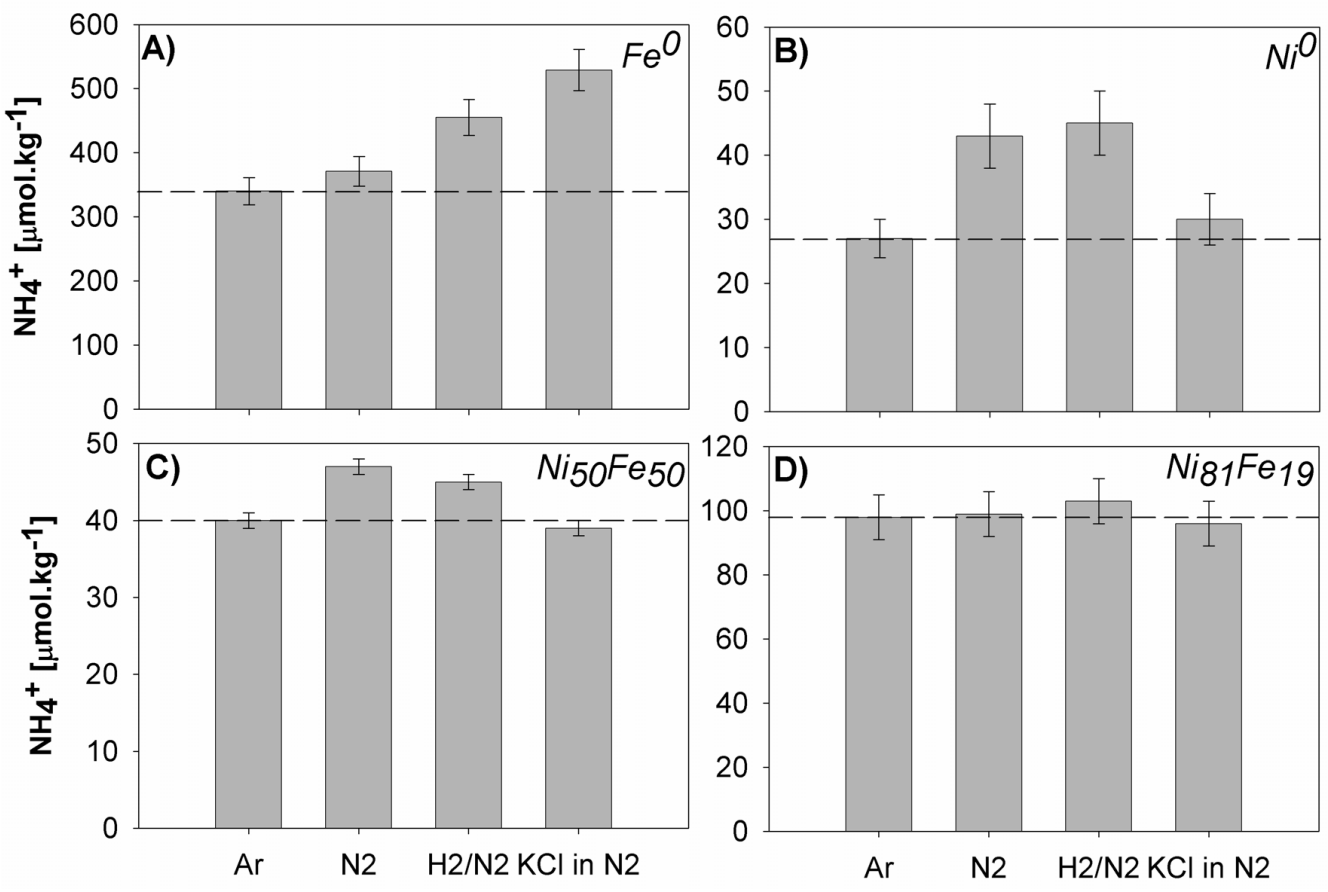

Figure 4
NH_4^+ formation from N_2 in the presence of Ni, Fe metals and alloys at 200°C. The dashed lines correspond to the Ar blank. The concentrations of KCl in the experiments were 459 μmol.kg^{-1} in A, B and 476 μmol.kg^{-1} in C, D. Results are normalized to 1 m^2 of surface area.

4a), followed by Ni^0 (16 μmol.kg^{-1}.m^2, Fig. 4b) and $Ni_{50}Fe_{50}$ (7 μmol.kg^{-1}.m^2, Fig. 4c). H_2(aq) was observed to form in the presence of all studied metals and alloys. Representative concentrations of H_2(aq) at 200°C (measured in one experiment with N_2-saturated, O_2-free DI per metal/alloy only) were 0.38 mmol.kg^{-1} with Ni^0, 0.28 mmol.kg^{-1} with $Ni_{81}Fe_{19}$, 0.7 mmol.kg^{-1} with $Ni_{50}Fe_{50}$ and 21 mmol.kg^{-1} with Fe^0. We point out that this H_2 production is relatively large compared to the background H_2 production of the Ti reaction vessels that was determined to be 12 μmol.kg^{-1} in an experiment with DI saturated with Ar at 200°C. An interesting observation during our experiments was that the reactivity of Fe^0 towards O_2-free DI was so rapid that gas bubbles were forming on its surface after just a few hours of exposure at 22°C (by analogy with 200°C experiments we assume it is H_2).

Our results showed that the addition of H_2 (5%/95% H_2/N_2) into the reaction mixture only resulted in change in the Fe^0 circumstance where 158 μmol.kg^{-1}.m^2 NH_4^+ was produced (Fig. 4a). Fe^0 was also the material most affected by the addition of K^+ (KCl). In this case, 189 μmol.kg^{-1}.m^2 of NH_4^+ was produced, 158 μmol.kg^{-1}.m^2 more than with N_2 alone (Fig. 4a). In general, our experiments showed that $Ni_{81}Fe_{19}$ was the least, and Fe^0, the most, affected by the addition of H_2 or KCl into the reacting solution (Fig. 4d, a).

Aqueous Fe and Ni cations ($NiCl_2$, $FeCl_2$) only had a small effect on N_2 reduction chemistry, converting about 1% of the total available N into NH_4^+ at 200°C (Tab. 1). A post-reaction visual inspection of the $FeCl_2$ solution showed a fine-grained colloid of reddish color that, in the presence of atmospheric O_2 changed color to light brown. The amount of recovered solids was insufficient for analysis by XRD.

At temperatures of 70 and 22°C no NH_4^+ formation from N_2 was observed (Tab 1, runs 38, 44, 50, 55, 61, 67, 73, 79). Use of these lower temperatures also resulted in

lower background NH_4^+ production in solutions containing the metals/alloys. The yield of NH_4^+ ranged from 7.4 (Fe^0) to 1.2 μmol.kg^{-1}.m^2 ($Ni_{50}Fe_{50}$) at 70°C (Tab. 1, runs 37, 43, 49, 54) and 1.4 (Fe^0) to 0 μmol.kg^{-1}.m^2 ($Ni_{50}Fe_{50}$, $Ni_{81}Fe_{19}$) at 22°C (Tab. 1, runs 60, 66, 72, 78).

Nitrite and nitrate reduction

The results of our NO_2^- and NO_3^- reduction experiments are shown in Fig. 5. At 200°C all tested metals/alloys were found to be very effective in converting NO_2^-/NO_3^- into NH_4^+. To assess if the presence of NO_2^- or NO_3^- in the solution had any effect on N_2 reduction, each experiment was conducted in duplicate with Ar (Tab. 1, runs 7, 8, 15, 16, 23, 24, 31, 32) and N_2 (Tab. 1, runs 5, 6, 13, 14, 21, 22, 29, 30) saturated solutions (e.g., Fe^0 with NO_2^-/N_2 and NO_2^-/Ar). These experiments taken in sum showed that there was no difference between the N_2 and Ar runs (Fig. 5a).

The results collected at 70°C reveal prominent differences between alloys and metals (Fig. 5b). While Ni and Fe achieved almost 100% conversions of NO_2^-/NO_3^- to NH_4^+ (Tab. 1, runs 40, 42, 46, 48), interestingly, no- or insignificant reduction (less than 20%) was observed in solutions reacted with alloys (Tab. 1, runs 51, 53, 57, 59). The presence of O_2 in the solution appears to have an inhibitive effect on the reduction process, especially in the presence of $Ni_{81}Fe_{19}$ alloy (Tab. 1, runs 56, 58; Fig. 5b).

Low temperature experiments (22°C) further confirmed the temperature dependence of NO_2^-/NO_3^- reduction in the presence of alloys (Fig. 5c). Compared to 200°C and even at 70°C, NH_4^+ formation was negligible (less than 1% conversion) (runs 63, 65, 69, 71, 75, 77, 81, 83). The effect of O_2 in the reacted solution was most pronounced with NO_3^- in the presence of Ni^0 (run 70). In general, at 22°C Fe^0 was the most efficient material in converting NO_2^-/NO_3^- to NH_4^+, regardless of the O_2 content (Tab. 1, runs 62–65; Fig. 5c).

It is important to note that at 200°C both NO_2^- and NO_3^- decomposed in the absence of metal/alloys as well (Tab. 1, runs 34, 34). 42% of the initial 497 μmol.kg^{-1} KNO_2 solution was converted into NO_3^- (~15%), NH_4^+ (~9%) and other N compounds (~18%) that were not analyzed. Of the initial 444 μmol.kg^{-1} KNO_3 solution, 71% was converted into NO_2^- (~61%), NH_4^+ (~1%) and about 9% corresponds to other unanalyzed N compounds. It is not clear if this is a result of thermally induced decomposition, catalysis or reaction by/with the titanium reaction vessel, or a combination of all; nevertheless, NH_4^+ was not the dominant reaction product. At 70 and 22°C, both NO_2^- and NO_3^- solutions were found to be stable in experiments without metals or alloys during the 24-hour reaction period.

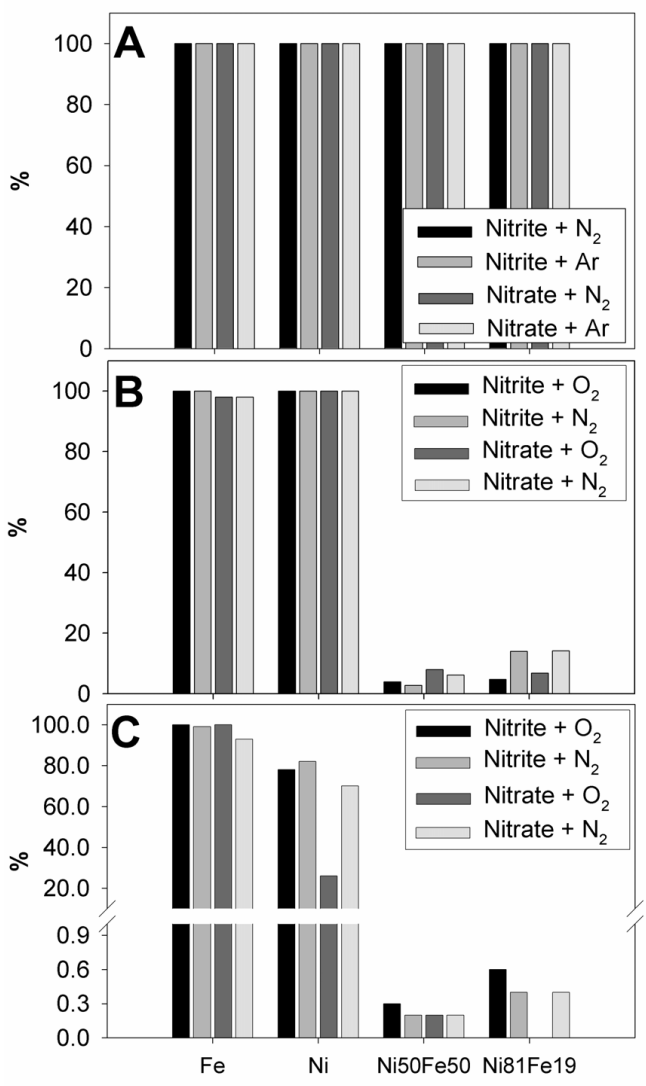

Figure 5
NH_4^+ formation from nitrite and nitrate, expressed in terms of % conversion. Panels A, B and C correspond to sets of experiments at 200, 70 and 22°C, respectively.

Metal/alloy alteration

Generally, the extent of alteration of Fe-containing metal/alloy increased with temperature, as demonstrated by the presence of secondary minerals (Fig. 6). Magnetite (Fe_3O_4) was the most abundant alteration product, predominantly forming euhedral to subhedral crystals up to several μm in size (Fig. 6a, b, d, e). Pseudomorphoses of magnetite after reacted spherical Fe^0 particles were common (Fig. 6d). The second most common alteration phase were Fe-(oxy)hydroxides (e.g., lepidocrocite) usually of amorphous appearance or forming needle-like (Fig. 6c) and platy crystals several tens of nm thin and several μm long. Both magnetite and Fe-(oxy)hydroxides commonly occur simultaneously in all reacted samples (SEM) (Fig.

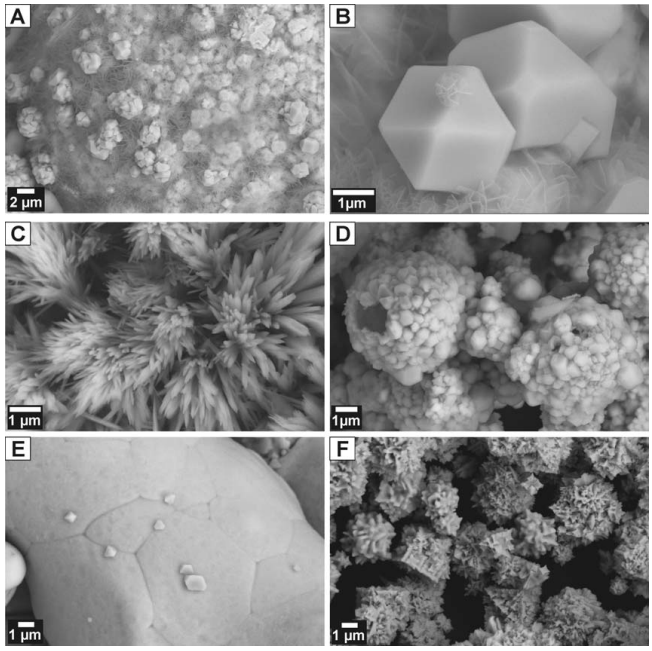

Figure 6
SEM microphotographs of reacted metals and alloys. A) Fe^0 reacted in N_2(aq) solution depicting coexisting magnetite and Fe-(oxy)hydroxides; B) Detail of magnetite single crystals formed on Fe^0; C) clusters of needle-like Fe-(oxy)hydroxide crystals formed on Fe^0; D) pseudomorphoses of magnetite after Fe^0 in the H_2/N_2 solution; E) magnetite crystals formed on $Ni_{50}Fe_{50}$ in the KNO_3 solution; F) Ni^0 skeletal crystal revealing no change after reaction.

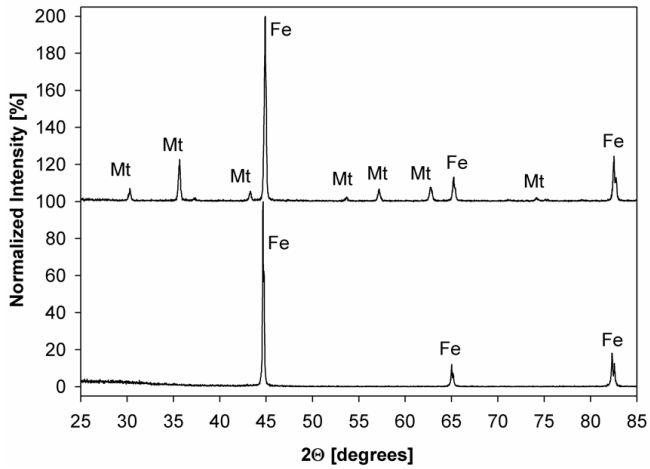

Figure 7
Normalized XRD patterns of unreacted (lower) reacted (upper) Fe^0 showing the presence of magnetite (Mt).

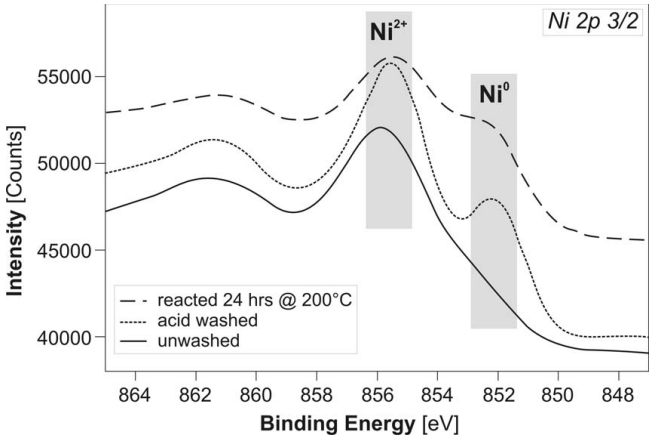

Figure 8
Ni 2p3/2 peaks showing the speciation of Ni on the surface Ni metal powder at various stages of the experiment. Note the presence of residual zerovalent Ni on the surface after 24 hour reaction at 200°C.

6a,b); however, only magnetite is identified by the XRD method (Fig. 7). This suggests that the Fe-(oxy)hydroxides either lack long range order (e.g., "X-ray amorphous") and/or their abundance is less than 5%, the approximate detection limit of XRD. In general, the lower the Fe content, the lower the extent of alteration (Fig. 6e). In contrast, reacted Ni^0 exhibited no microscale (SEM) evidence of reaction (Fig. 6f, compare with Fig. 3a), as corroborated by the XPS spectra documenting the presence of residual zero-valent Ni species on the surface (Fig. 8). As a result of solution interactions with metals/alloys, the resulting pH in most experiments was higher than the starting value (see discussion) (Tab. 1).

Discussion

Nitrogen in alloys and metals

All the metals and alloys investigated in this work were found to contain N, which resulted in a background production of NH_4^+. The presence of atomic N was based on two lines of evidence: 1) The presence of the N1s peak in the XPS spectra of starting metals and alloys even after "cleaning" the surface by sputtering with Ar^+ ions (Fig. 9) and; 2) quantitative analysis of N_{tot} content of the starting materials by inert gas fusion with a thermal conductivity detection (Tab. 3).

Commercially available Ni, Fe metals/alloys may contain N due to the manufacturing process which employs either inert (N_2, Ar) or reducing (NH_3, H_2) atmospheres to prevent oxidation [38,39] [Alfa Aesar, Goodfellow – pers.comm]. For example, during the synthesis, N_2 chemisorbs on the surface of molten/hot metal and dissociates (Equation 1).

$$N_2\,(\text{gas}) \rightarrow 2N\,(\text{in metal}) \qquad (1)$$

Table 3: Total N content of metals and alloys used in this study as determined by inert gas fusion – thermal conductivity method (IMR Test Labs).

Sample	N_{TOTAL} [wt.%]
Fe^0	0.0124 ± 0.001
Ni^0	0.0012 ± 0.0005
$Ni_{50}Fe_{50}$	0.0030 ± 0.0005
$Ni_{81}Fe_{19}$	0.0009 ± 0.0005

In the subsequent step N enters the structure via diffusion or convection to form primarily monoatomic interstitial and to lesser extent substitutional solid solutions. This process is governed by the Sievert's law (Equation 2), which predicts that diatomic gases such as N_2 dissolve in metals (c_N) proportionally to the square root of the partial pressure (p_{N2}) in the coexisting gas phase [40,41].

$$K = \frac{c_N^2}{p_{N_2}} \quad (2)$$

Assuming homolytic N_2 bond cleavage, each N atom would have three unpaired electrons available for bonding with the surrounding metal atoms. XPS spectra collected from unreacted metals/alloys in our experiments point to nitride (N^{3-}, 398.6 eV) as the likely N species (Fig. 9) [42]. Consequently, upon release into the solution, N^{3-} is expected to react with available protons to form NH_3/NH_4^+ (Reaction 3, 4) and contribute to their high background productivity.

$$N^{3-} + 3H^+ \rightarrow NH_3 \quad (3)$$

$$N^{3-} + 4H^+ \rightarrow NH_4^+ \quad (4)$$

However, undissociated N_2 gas may get trapped in the molten metal (e.g., in inclusions) as well.

Dinitrogen reduction

Although batch-type experiments, such as the ones described above, provide little insight into the kinetics of a reaction and much less the reaction mechanism, the results do allow one to compare the amount of NH_3/NH_4^+ formed under different conditions. In addition the results can be placed in the context of previously published research related to the reduction of N-species to NH_3/NH_4^+. Due to the immense importance of NH_3/NH_4^+ in industry and agriculture, several decades of research exist on its synthesis and production from N_2 gas [e.g., [43]]. The industrial Haber-Bosch process utilizes Fe^0 catalyst at high temperatures and pressures (~500°C, ~100 bars) to synthesize NH_3 from H_2 and N_2 gas (Reaction 5).

$$N_2(g) + 3H_2(g) \rightarrow 2NH_3(g) \quad (5)$$

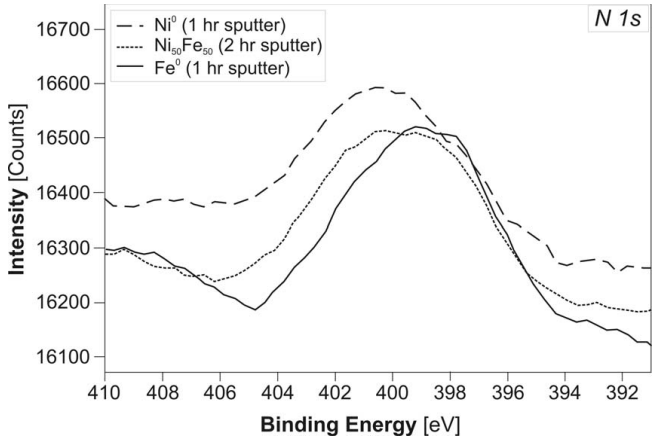

Figure 9
N 1 s peaks centered around 400 eV documenting the presence of N in the tested alloys and metals after sputtering with Ar^+ (Ni^0 400.1 eV, $Ni_{50}Fe_{50}$ 399.7 eV, Fe^0 398.9 eV).

In brief, the reaction proceeds as follows: sorption of H_2 and N_2 gases on the surface is followed by the formation of atomic H_{ads} and N_{ads} (dissociative sorption). Fe^0 then facilitates electron transfer from H_{ads} to N_{ads} (e.g., N reduction), followed by the formation of NH_3 gas on the surface and subsequent desorption. The dissociative chemisorption of N_2 is generally taken to be the rate-limiting step [44]. For comparison, modern life overcomes the reaction's activation barrier using the enzyme *nitrogenase* composed of dinitrogenase (MoFe center) and dinitrogenase reductase (Fe center) proteins. In Reaction 6, Fd stands for ferredoxin, the electron-transfer protein [45,46].

$$N_2(g) + 8Fd^0_{red} + 10H^+ \rightarrow 2NH_4^+ + 8Fd^+_{ox} + H_2(g) \quad (6)$$

Analogous overall reactions of abiotic N_2 reduction can be written for aqueous solutions (Reaction 7, 8), although it is important to note that since this reaction requires a transfer of multiple electrons, several reaction intermediates must be involved. Once in solution, NH_3 and NH_4^+ exist in a pH dependent equilibrium (Equation 9; valid for 25°C).

$$N_2(aq) + 2H^+ + 3H_2(aq) \rightarrow 2NH_4^+ \quad (7)$$

$$N_2(aq) + 3H_2(aq) \rightarrow 2NH_3(aq) \quad (8)$$

$$pH = 9.25 + \log\left\{\frac{[NH_3]}{[NH_4^+]}\right\} \quad (9)$$

We hypothesize that reactions between H_2, N_2 and the metal/alloy surface are taking place in our experiments;

Table 4: Predicted equilibrium pH and nitrogen speciation in the N-H_2O-Fe-Ni system (only species with molalities above $1{\cdot}10^{-8}$ shown). Concentrations and fugacities of dominant N species are in bold. The last column shows the predicted final mineral assemblage.

Mineral	*T [°C]*	*pH*	mNH_3	mNH_4^+	mN_2	mH_2	fNH_3	fN_2	fH_2	*Assemblage*
Nickel	200	6.95	$\mathbf{6.4{\cdot}10^{-4}}$	$4.63{\cdot}10^{-5}$	$2.47{\cdot}10^{-4}$	$3.73{\cdot}10^{-5}$	$1.24{\cdot}10^{-3}$	**0.2769**	0.24	BN, NI
Nickel	70	8.92	$\mathbf{1.00{\cdot}10^{-3}}$	$1.34{\cdot}10^{-4}$	$2.2{\cdot}10^{-5}$	$2.68{\cdot}10^{-7}$	$9.98{\cdot}10^{-5}$	**0.0477**	$3.68{\cdot}10^{-4}$	BN, NI
Nickel	22	10.2	$\mathbf{1.03{\cdot}10^{-3}}$	$1.34{\cdot}10^{-4}$	$8.12{\cdot}10^{-6}$	$2.18{\cdot}10^{-8}$	$1.41{\cdot}10^{-5}$	**0.0118**	$2.71{\cdot}10^{-5}$	BN, NI
Awaruite	200	7.07	$\mathbf{1.12{\cdot}10^{-3}}$	$6.14{\cdot}10^{-5}$	$<1{\cdot}10^{-8}$	0.0597	$\mathbf{2.16{\cdot}10^{-3}}$	$<1{\cdot}10^{-8}$	38.54	AW, MT, NI
Awaruite	70	8.93	$\mathbf{1.04{\cdot}10^{-3}}$	$1.37{\cdot}10^{-4}$	$<1{\cdot}10^{-8}$	0.0152	$\mathbf{1.04{\cdot}10^{-4}}$	$<1{\cdot}10^{-8}$	20.85	AW, MT, NI
Awaruite	22	10.2	$\mathbf{1.05{\cdot}10^{-3}}$	$1.35{\cdot}10^{-4}$	$<1{\cdot}10^{-8}$	0.0103	$\mathbf{1.44{\cdot}10^{-5}}$	$<1{\cdot}10^{-8}$	12.82	AW, MT, NI
Tetrataenite	200	8.7	$\mathbf{5.92{\cdot}10^{-4}}$	$7.96{\cdot}10^{-7}$	$<1{\cdot}10^{-8}$	0.0865	$\mathbf{1.14{\cdot}10^{-3}}$	$<1{\cdot}10^{-8}$	55.85	AW, MT, TT
Tetrataenite	70	8.93	$\mathbf{1.04{\cdot}10^{-3}}$	$1.37{\cdot}10^{-4}$	$<1{\cdot}10^{-8}$	0.0222	$\mathbf{1.04{\cdot}10^{-4}}$	$<1{\cdot}10^{-8}$	30.51	AW, MT, TT
Tetrataenite	22	10.2	$\mathbf{1.05{\cdot}10^{-3}}$	$1.35{\cdot}10^{-4}$	$<1{\cdot}10^{-8}$	0.0159	$\mathbf{1.44{\cdot}10^{-5}}$	$<1{\cdot}10^{-8}$	19.73	AW, MT, TT
Iron	200	7.07	$\mathbf{1.15{\cdot}10^{-3}}$	$6.22{\cdot}10^{-5}$	$<1{\cdot}10^{-8}$	1.532	$\mathbf{2.22{\cdot}10^{-3}}$	$<1{\cdot}10^{-8}$	989.1	MT, FE
Iron	70	8.93	$\mathbf{1.06{\cdot}10^{-3}}$	$1.38{\cdot}10^{-4}$	$<1{\cdot}10^{-8}$	0.785	$\mathbf{1.05{\cdot}10^{-4}}$	$<1{\cdot}10^{-8}$	1077	MT, FE
Iron	22	10.2	$\mathbf{1.06{\cdot}10^{-3}}$	$1.36{\cdot}10^{-4}$	$<1{\cdot}10^{-8}$	0.623	$\mathbf{1.45{\cdot}10^{-5}}$	$<1{\cdot}10^{-8}$	771.5	MT, FE
Goethite	200	5.59	$<1{\cdot}10^{-8}$	$<1{\cdot}10^{-8}$	$\mathbf{5.86{\cdot}10^{-4}}$	$<1{\cdot}10^{-8}$	$<1{\cdot}10^{-8}$	**0.6574**	$<1{\cdot}10^{-8}$	HM
Goethite	70	6.1	$<1{\cdot}10^{-8}$	$<1{\cdot}10^{-8}$	$\mathbf{5.86{\cdot}10^{-4}}$	$<1{\cdot}10^{-8}$	$<1{\cdot}10^{-8}$	**1.273**	$<1{\cdot}10^{-8}$	HM
Goethite	22	6.22	$<1{\cdot}10^{-8}$	$<1{\cdot}10^{-8}$	$\mathbf{5.86{\cdot}10^{-4}}$	$<1{\cdot}10^{-8}$	$<1{\cdot}10^{-8}$	**0.8475**	$<1{\cdot}10^{-8}$	HM
Magnetite	200	6.08	$1.04{\cdot}10^{-5}$	$5.42{\cdot}10^{-6}$	$\mathbf{5.82{\cdot}10^{-4}}$	$1.79{\cdot}10^{-6}$	$2.0{\cdot}10^{-5}$	**0.653**	$1.16{\cdot}10^{-3}$	HM, MT
Magnetite	70	8.47	$1.26{\cdot}10^{-4}$	$4.73{\cdot}10^{-5}$	$\mathbf{5.04{\cdot}10^{-4}}$	$2.36{\cdot}10^{-8}$	$1.25{\cdot}10^{-5}$	**1.094**	$3.24{\cdot}10^{-5}$	HM, MT
Magnetite	22	9.97	$3.1{\cdot}10^{-4}$	$7.35{\cdot}10^{-5}$	$\mathbf{3.98{\cdot}10^{-4}}$	$<1{\cdot}10^{-8}$	$4.26{\cdot}10^{-6}$	**0.5759**	$3.32{\cdot}10^{-6}$	HM, MT
Ferrihydrite	200	5.59	$<1{\cdot}10^{-8}$	$<1{\cdot}10^{-8}$	$\mathbf{5.81{\cdot}10^{-4}}$	$<1{\cdot}10^{-8}$	$<1{\cdot}10^{-8}$	**0.6512**	$<1{\cdot}10^{-8}$	HM
Ferrihydrite	70	6.1	$<1{\cdot}10^{-8}$	$<1{\cdot}10^{-8}$	$\mathbf{5.81{\cdot}10^{-4}}$	$<1{\cdot}10^{-8}$	$<1{\cdot}10^{-8}$	**1.261**	$<1{\cdot}10^{-8}$	HM
Ferrihydrite	22	6.22	$<1{\cdot}10^{-8}$	$<1{\cdot}10^{-8}$	$\mathbf{5.81{\cdot}10^{-4}}$	$<1{\cdot}10^{-8}$	$<1{\cdot}10^{-8}$	**0.8396**	$<1{\cdot}10^{-8}$	HM

Abbreviations: BN = bunsenite, NI = Ni metal, AW = awaruite, MT = magnetite, TT = tetrataenite, FE = Fe metal, HM = hematite.

however, they are orders of magnitude slower than those described above in the gas phase. Undoubtedly, this is due to the fact that aqueous reactions occurring in our experiments are not only more complex but also take place at much lower *T*, *P* conditions and H_2/N_2 concentrations than those typical for Haber-Bosch synthesis. Such kinetic constraints could explain low NH_4^+ yields, even though the thermodynamic equilibrium models predict NH_4^+ to be the dominant N species (Tab. 4).

We speculate that in the presence of Fe^0 most of the NH_4^+ was rapidly formed in the first few hours of the experiment when unreacted surface was still available for reaction. In this scenario (e.g., run 2) most (and possibly all) H_2 is formed *in situ* as a result of interactions between the pristine Fe^0 surface and H_2O (Reaction 10) (e.g., $mH_2 = 0$ at t_0); however, the simultaneous Fe oxidation passivates the surface, reduces the availability of suitable H_2/N_2 sorption sites and the overall yield of the N_2-reduction reaction.

$$Fe + 2H_2O \rightarrow H_2 + Fe^{2+} + 2OH^- \qquad (10)$$

This notion is corroborated by experiments carried out with conditions in which H_2 was present in the system from the start of the reaction (e.g., run 3), as a result of purging the solution with a H_2/N_2 mixture prior to loading (e.g., $mH_2 > 0$ at t_0). Abundant H_2 in this run correlates with greater NH_4^+ production as the overall N_2 conversion rate increases from 2.5 to 10% (Tab. 2). Assuming that in both cases Fe^0 surface passivates at the same rate, then the H_2 purged system produces more NH_4^+ per unit of time because it does not depend on the Fe^0 alteration process (Reaction 10) to provide H_2. This circumstance may be more typical of natural serpentinization-driven SHS where H_2 can be provided by a number of processes, especially by Fe^{2+} oxidation during alteration of rock-forming silicates [17,47].

Similar assumptions can be made about $Ni_{50}Fe_{50}$ and $Ni_{81}Fe_{19}$ assuming that Fe atoms exposed on the surface played a role in the reduction process. Due to good corrosion resistance, Ni^0 reacted to a much lesser extent and consistent with this lower activity is our experimental observation that the Ni^0 surface was not significantly altered (e.g., by precipitation of neoformed phases) throughout the experiment. Different modes of metal/alloy participation in studied reactions are discussed below.

The addition of KCl into the Fe^0-H_2O-N_2 system in our experiments resulted in higher NH_4^+ yield (Fig. 4a). While it may be intriguing to draw parallels with the Haber-Bosh process, where K is added to improve sticking coefficients and to help stabilize sorbed species [44], the apparent promoting effect of KCl may be partially or entirely caused

by the presence of chloride ion (Cl^-) in the solution. Cl^- can react with dissolved iron in the solution (Reaction 11) and remove products from the Fe^0 dissolution reaction (Reaction 10).

$$Fe^{2+} + 2Cl^- \rightarrow FeCl_2 \quad (11)$$

Such a complexation reaction would result in an equilibrium shift towards the product side and further drive the dissolution process and release of structurally bound reduced N species into the solution (Reactions 3, 4). This is in agreement with the results of Reardon [48] who observed an increase in Fe^0 corrosion rates in low ionic strength (~0.02 *m*) anaerobic NaCl, $NaHCO_3$ and Na_2SO_4 solutions compared to DI water. The NH_4^+ content of the KCl reagent solution at concentrations used in our experiments was found to be below the detection limit of ion chromatography.

Nitrite and Nitrate Reduction

Due to their status as environmental contaminants, NO_2^-/NO_3^- reduction has been extensively studied, especially focused on the reduction of NO_3^- by Fe^0. Most of the published results concur that the reduction reaction (Reaction 12) at anaerobic ambient conditions exhibits the following set of features: 1) reaction rates decrease with increasing pH; 2) pH in unbuffered solutions becomes more alkaline as the reaction progresses; 3) NH_4^+ and Fe_3O_4 are the dominant reaction products; 4) NO_3^- reduction slows down once Fe^0 is coated with Fe_3O_4 unless Fe^{2+}, Cu^{2+}, Al^{3+} or Fe^{3+} are present; 5) SO_4^{2-} inhibits the reaction; and 6) the molar N_2:NH_4^+ ratio in reaction products increases with pH [49-57].

$$4Fe^0 + 10H^+ + NO_3^- \rightarrow NH_4^+ + 4Fe^{2+} + 3H_2O \quad (12)$$

$$3Ni_3Fe + 4NO_2^- + 24H_2O \rightarrow 32OH^- + 4NH_4^+ + 3Fe^{2+} + 9Ni^{2+} \quad (13)$$

Analogous reactions can be written for other metals/alloys as well as NO_2^- (Reaction 13), although they have been by comparison less studied. The absence of resonance structures in the NO_2^- molecule makes it easier to reduce than NO_3^- [58], which is reflected in reduction reaction rates. For example, NO_3^- reduction to NH_4^+ in the presence of Fe^{2+} was found to be a factor of 8 slower than that of NO_2^- [5]. Because the reduction from NO_3^- to NH_4^+ requires transfer of at least 8 electrons, several intermediates must be formed in the process. Moreover, the formation of any N-N bonds must be avoided because it is effectively inert under all but the highest temperatures investigated here.

It is widely recognized, however, that NO_2^- is a reaction intermediate in NO_3^- reduction [e.g., [51]] [57,59]. For example, Wärna *et al* [59] proposed a reaction sequence from NO_3^- and NO_2^- through nitric oxide (NO), imidogen (HN) and aminyl radical ($H_2N^{\cdot}$) to NH_3/NH_4^+ on the surface of Fe^0. Several studies with NO_2^-/NO_3^- as well as some organic compounds suggest that Fe^{2+}, Fe^0, and Fe^{2+} sorbed on neoformed Fe minerals (e.g., magnetite) are likely electron donors for the reduction reactions [e.g., [60]] [61,62]. The intriguing consequence of such a reaction mechanism in natural systems is that precipitation of secondary (neoformed) Fe minerals further along the flow path followed by surface sorption of Fe^{2+} would provide additional reaction sites for the reduction of NO_2^-/NO_3^- [e.g., [63]].

The role of alloys/metals

Based on the XPS (oxidation state of Ni) and SEM (abundance of Fe- and the absence of Ni alteration phases) results it is possible to construct an order of apparent stability of studied alloys and metals

$$Ni^0 > Ni_{81}Fe_{19} > Ni_{50}Fe_{50} > Fe^0$$

where Ni^0 is most- and Fe^0 is least stable under the studied experimental conditions. This enables us to generalize that the higher the Fe content, the higher the reactivity towards potential oxidizing agents (e.g., H_2O, NO_2^-, NO_3^-) and thus the higher extent of alteration. Metals and alloys typically undergo reductive dissolution (e.g., Reaction 10); however alloys frequently dissolve the less noble metal preferentially, leaving the surface enriched in the more noble metal [e.g., [64]]. For example, the reductive dissolution of $Ni_{50}Fe_{50}$ alloys is expected to result in preferential release of Fe and a concomitant increase in the Ni:Fe ratio of the residual alloy.

Our findings are in agreement with metallurgical studies in which it has been demonstrated that Ni^0 is more corrosion resistant than Fe^0, a notion that serves as a basis for their frequent alloying [38,65]. Unlike Fe^0, Ni^0 reacts to a lesser degree in aqueous environments (reaction produces H_2 and Ni^{2+}), especially under reducing conditions. The presence of an oxidizing agent is usually required for significant corrosion; however, a protective oxide film may develop and impede further reactions [38,66]. Ni^0 with a combination of catalytic properties and corrosion resistance (e.g., slow dissolution kinetics) may serve as a basis for a unique mechanism of N_2 reduction, where Ni acts both as a reactant and a catalyst. We hypothesize that Ni^0 reacts with H_2O to produce H_2, a portion of which may stay adsorbed on the surface in its atomic form (H_{ads}) (Reaction 14). If N_2 is also dissociatively chemisorbed (Reaction 15), surface-mediated reduction reactions may proceed (Reaction 16).

$$Ni + 2H_2O \rightarrow 2H_{ads} + Ni^{2+} + 2OH^- \quad (14)$$

$$N_2(aq) \rightarrow 2N_{ads} \quad (15)$$

$$2N_{ads} + 2H^+ + 6H_{ads} \rightarrow 2NH_4^+ \quad (16)$$

This set of reactions may operate until all plausible sorption sites are exhausted and/or deactivated. By analogy, we argue that if the experimental conditions were approaching the stability field of Fe metal (e.g., at sufficiently high fH_2) it could behave in a similar manner.

There exist; however, "true" catalytic systems for NO_2^-/NO_3^- reduction, such as bimetallic Cu-Pt and Cu-Pd, Ag-Pd, Ag-Pt, which couple a noble metal and an oxidizable promoter. The reactions take place on the surface of Cu^0 which acts as an electron donor for the reduction of N species and as an acceptor of electrons from dissociative sorption of H_2 on the surface of Pt [67,68]. Even though natural alloys of platinum group elements (Pt, Pd, Ir, Os, Rh, Ru) are scarce on modern Earth and are almost exclusively limited to magmatic segregation deposits, placers, and meteorites [e.g., [69]] [70,71], their significance for prebiotic synthesis should not be overlooked [72].

The predominantly alkaline pH in reacted samples (Tab. 2) is likely a result of several pH controlling reactions such as reductive dissolution of metals (e.g., Reaction 10), mineral formation (e.g., magnetite), and the buffering reactions involving charged species including, but not limited to NO_3^-, NO_2^-, NH_3, or NH_4^+. The fate of Fe^{2+} in the experiments reported here is difficult to constrain. Assuming completely anoxic conditions, temperatures below 85°C and a negligible pCO_2 in our experiments, $Fe(OH)_2$ (white rust) could precipitate (Reaction 17) and due to its instability serve as a precursor to other Fe oxides and hydroxides, most notably Fe_3O_4 (Reaction 18).

$$Fe^{++} + 2OH^- \rightarrow Fe(OH)_2 \quad (17)$$

$$3Fe(OH)_2 \rightarrow Fe_3O_4 + 2H_2O + H_2 \quad (18)$$

At higher temperatures and/or in the presence of trace levels of O_2 or other oxidizing agents (e.g., NO_3^-), mineral intermediates such as green rust (mixed-valence hydroxide) may have been involved [e.g., [73]] [74,75].

The conversion of the original metal/alloy into a new mineral phase (e.g., coatings) may not necessarily negatively affect the NH_3/NH_4^+ production. For example, wüstite (FeO) and green rust – both possible reaction products/intermediates during anaerobic Fe^0 oxidation, have been shown to reduce NO_2^-/NO_3^- [e.g., [50]] [76-78]. Magnetite and even goethite can also act as reductants for NO_2^-/NO_3^-, provided cations such as Fe^{2+}, Cu^{2+}, Fe^{3+}, Al^{3+} are present in the system [e.g., [53]] [56,79]. Equilibrium thermodynamic calculations, however, predict very little reactivity of magnetite, goethite, or ferrihydrite alone towards N_2 and anaerobic experiments in the presence of green rust at ambient T, p conditions corroborate these predictions [80].

Implications for the Hadean Earth

Different modes of metal/alloy participation have different implications for natural systems, especially in terms of the amount of metal/alloy required to achieve the same NH_3/NH_4^+ production. A catalyst remains stable during the reaction and therefore a small amount can, in theory, catalyze the formation of large amounts of NH_3/NH_4^+. Conversely, a reactant would have to be present in sufficient amounts and/or would have to be continually formed in order to achieve comparable NH_3/NH_4^+ production. While both mechanisms are plausible on the Hadean Earth, it is hard to assess which of the two would be prevalent. Based of equilibrium geochemical modeling, Smirnov [28] concluded that at 200°C Ni metal is stable at fH_2 orders of magnitude lower than Fe metal and even $Ni_{50}Fe_{50}$ (tetrataenite) and $Ni_{81}Fe_{19}$ (awaruite). Combined with results acquired from this study, it would appear that Ni metal is the most suitable candidate for a sustained long-term NH_3/NH_4^+ formation. Moreover, if we consider that the Hadean atmosphere may have had up to 30% H_2 [29], the primordial ocean would contain significantly higher concentrations of dissolved H_2 than today. In SHS, H_2 from advected seawater combined with H_2 formed by serpentinization could create conditions sufficiently reducing for stabilization of Fe containing alloys (e.g., awaruite, tetrataenite) and possibly even Fe^0. Furthermore, as shown by Schoonen et al [72], seawater trapped in closed SHS (i.e., not open to seawater circulation) evolves to become extremely reduced as the partial pressure of hydrogen builds up.

The possibility of hydrothermal reduction of N_2 to NH_4^+ permits us to attempt to constrain the total NH_4^+ flux from Hadean off-axis SHS. The following set of assumptions and variables were taken into account:

1) The total heat production of the Hadean Earth was several times higher than today [81,82]. Because the exact value is unknown, we calculated scenarios for 2- to 8-times the present day heat flow (PDHF = 4.3×10^{13} W) [83] (Fig. 10); however, only values between 4 and 8 times PDHF are reported.

2) Because it is unclear if a global tectonic cycle was operational during the Hadean, we are unable to comment on the dissipation of Earth's internal heat, especially on the percentage of heat released through SHS. Therefore, two endmember scenarios are considered: a) heat is dissipated predominantly via volcanism (possibly through several supervolcanoes) and only 5% is released through hydro-

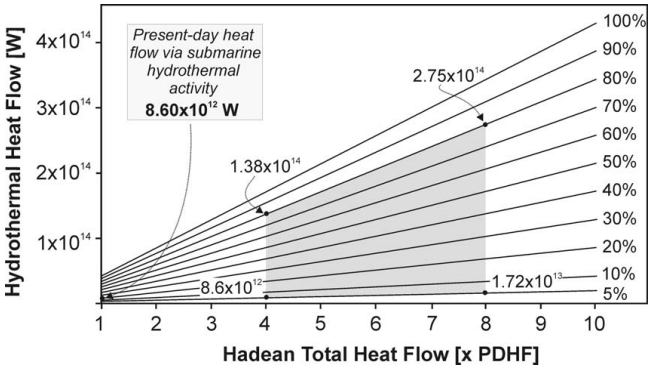

Figure 10
Hadean hydrothermal flow as a function of total Earth's heat flow (expressed as multiplicities of present day heat flow – PDHF). Each data line thus represents percentage of the total heat flow released through hydrothermal systems at a given value of Hadean heat flow. The shaded area represents assumed realistic scenarios for the Hadean.

thermal activity; and b) 80% of heat is dissipated predominantly through hydrothermal activity (Fig. 10). For comparison, presently about 20% of PDHF is released through hydrothermal activity [83].

3) Due to the increased heat flow and possibly due to the blanketing effect of the atmosphere [e.g., [84]], we assume the mean ocean water temperature to be 70°C. Although modern serpentinization-driven SHS commonly vent fluids below 100°C [85-87], we assume that the higher overall heat flow in the Hadean would also increase the fluid temperature of hydrothermal vents [e.g., [88]]. The temperature of the discharging fluid is thus assumed to be 200°C for the purpose of this calculation. Although the temperature of ambient seawater and of discharging fluid directly influences the total hydrothermal fluid mass flux (equation 19), their variations (± 20°C) only produced small changes in the final NH_4^+ fluxes (usually within the same order of magnitude; data not shown). The heat capacity (c_p) of hydrothermal seawater at 200°C and P ~100–600 bar is 4.1 $J.g^{-1}K^{-1}$[89].

4) Ocean water is assumed to be in equilibrium with 1 bar of N_2, resulting in a dissolved N_2(aq) concentration of 0.481 $mmol.kg^{-1}$ at 70°C [90]. For simplicity, no other gases and/or aqueous ions were taken into consideration.

5) Even though experimental results reported in this study suggest a conversion of N_2-to-NH_4^+ 0.2 to 2.5% we calculate a variety of scenarios ranging from 0.1% to 10%. Although the 10% conversion may appear overly optimistic, our experiments suggest that the presence of advected H_2 and or K^+ may significantly improve the NH_4^+ production (Tab. 2; Fig. 4a). Metals/alloys may act as either catalysts or reactants, however, if metals/alloys do react, it must be assumed that the rate of their destruction (e.g., passivation, poisoning) is equal to their rate of formation (e.g., via serpentinization). It is important to point out that for simplicity, we do not distinguish between respective metals/alloys and we are only concerned with their capability to facilitate the conversion of N_2 to NH_4^+ (in %).

Table 5: Total N content of four octahedrites analyzed by inert gas fusion (IMR Test Labs).

Sample	N_{TOTAL} [wt.%]
Bogou Meteorite	0.0032 ± 0.0005
N'Goureyma Meteorite	0.0022 ± 0.0005
Sikhote Alin Meteorite	0.0032 ± 0.0005
Canyon Diablo Meteorite	0.0022 ± 0.0005

The mass flux of seawater through hydrothermal systems (F) can be estimated from heat flux (H) in Watts, heat capacity of seawater (c_p at 200°C) in $J.g^{-1}K^{-1}$ and temperature anomaly ΔT in Kelvin [83]:

$$F = \frac{H}{c_p \Delta T}. \quad (19)$$

Using hydrothermal heat fluxes from Fig. 10 we can calculate annual seawater mass fluxes from SHS. Subsequently, using various N_2-to-NH_4^+ conversion percentages (0.1 to 10%), annual NH_4^+ production of Hadean SHS is calculated (Fig. 11). Assuming the most conservative scenario with 0.1% conversion of N_2 to NH_4^+, the annual NH_4^+ production would be between 5.9 × 10^8 mol (4 × PDTH)

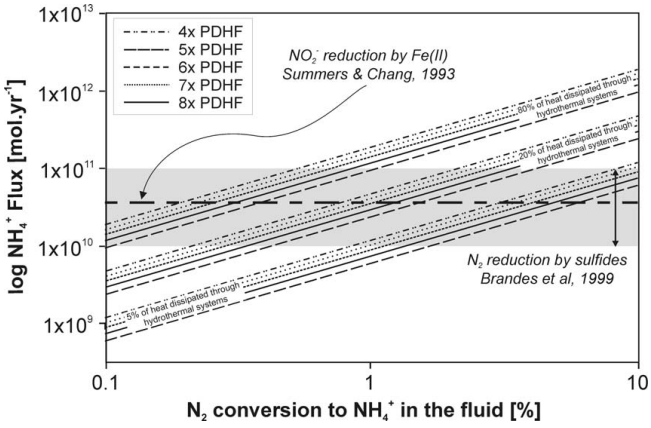

Figure 11
NH_4^+ formation from N_2 in Hadean hydrothermal systems. Fluxes are calculated as a function of N_2 conversion between 1 and 10%. NH_4^+ formation from NO_2^-/NO_3^- is not included in these calculations.

Table 6: NH_4^+ formation from N_2 in Hadean hydrothermal systems. Fluxes (mol.kg^{-1}.yr^{-1}) are calculated as a function of N_2 conversion between 1 and 10%. Note that NH_4^+ formation from NO_2^-/NO_3^- is not included in these calculations.

5% of Earth's heat flow is released via hydrothermal activity					
N_2 conversion	*Hadean heat flow (× PDHF)*				
%	4	5	6	7	8
0.1	5.9×10^8	7.3×10^8	8.8×10^8	1.0×10^9	1.2×10^9
0.5	2.9×10^9	3.7×10^9	4.4×10^9	5.1×10^9	5.9×10^9
1	5.94×10^9	7.3×10^9	8.8×10^9	1.0×10^{10}	1.2×10^{10}
2	1.2×10^{10}	1.5×10^{10}	1.8×10^{10}	2.1×10^{10}	2.4×10^{10}
5	2.9×10^{10}	3.7×10^{10}	4.4×10^{10}	5.1×10^{10}	5.9×10^{10}
10	5.9×10^{10}	7.3×10^{10}	8.8×10^{10}	1.0×10^{11}	1.2×10^{11}
20% of Earth's heat flow is released via hydrothermal activity					
N_2 conversion	*Hadean heat flow (× PDHF)*				
%	4	5	6	7	8
0.1	9.4×10^9	1.2×10^{10}	1.4×10^{10}	1.7×10^{10}	1.9×10^{10}
0.5	4.7×10^{10}	5.9×10^{10}	7.1×10^{10}	8.2×10^{10}	9.4×10^{10}
1	9.5×10^{10}	1.2×10^{11}	1.4×10^{11}	1.7×10^{11}	1.9×10^{11}
2	1.9×10^{11}	2.4×10^{11}	2.8×10^{11}	3.3×10^{11}	3.8×10^{11}
5	4.7×10^{11}	5.9×10^{11}	7.1×10^{11}	8.2×10^{11}	9.4×10^{11}
10	9.4×10^{11}	1.2×10^{12}	1.4×10^{12}	1.7×10^{12}	1.9×10^{12}
80% of Earth's heat flow is released via hydrothermal activity					
N_2 conversion	*Hadean heat flow (× PDHF)*				
%	4	5	6	7	8
0.1	9.4×10^9	1.2×10^{10}	1.4×10^{10}	1.7×10^{10}	1.9×10^{10}
0.5	4.7×10^{10}	5.9×10^{10}	7.1×10^{10}	8.2×10^{10}	9.4×10^{10}
1	9.5×10^{10}	1.2×10^{11}	1.4×10^{11}	1.7×10^{11}	1.9×10^{11}
2	1.9×10^{11}	2.4×10^{11}	2.8×10^{11}	3.3×10^{11}	3.8×10^{11}
5	4.7×10^{11}	5.9×10^{11}	7.1×10^{11}	8.2×10^{11}	9.4×10^{11}
10	9.4×10^{11}	1.2×10^{12}	1.4×10^{12}	1.7×10^{12}	1.9×10^{12}

and 1.2×10^9 mol (8 × PDTH) if 5% of Earth's heat is removed via SHS and between 9.4×10^9 mol (4 × PDTH) and 1.9×10^{10} mol (8 × PDTH) if 80% of heat is removed via SHS. Conversely, with a 10% N_2 conversion efficiency, the annual NH_4^+ production would be between 5.9×10^{10} mol (4 × PDTH) and 1.2×10^{11} mol (8 × PDTH) if 5% of heat is removed via SHS and between 9.4×10^{11} mol (4 × PDTH) and 1.9×10^{12} mol (8 × PDTH) if 80% of heat is removed by SHS (Tab. 5). To place these modeled fluxes in context we can compare their magnitude to those of other proposed NH_3/NH_4^+ formation mechanisms (Fig. 11). An annual NH_4^+ flux at 1% conversion efficiency, for example, would be comparable to that based on a homogeneous reaction (Reaction 20) of Summers and Chang [4] or to the flux calculated by Brandes *et al* [13], which was based on NH_3 formation in the presence of various minerals between 300 and 800°C.

$$6Fe^{2+} + 7H^+ + NO_2^- \rightarrow 6Fe(III) + 2H_2O + NH_3 \quad (20)$$

Although we cannot comment on the total NH_4^+ content of the Hadean Ocean, we can estimate the contribution of hydrothermal N_2 reduction per unit of time. For timescales longer than 1 year, the following equation may be used (21):

$$NH_4^+ \text{ addition to the ocean} = \frac{\text{annual } NH_4^+ \text{ production}}{V_{\text{Hadean Ocean}}} \bullet t. \quad (21)$$

NH_4^+ production in mol.yr^{-1} can be taken from Fig. 11 or Tab. 6 (or supplied from reader's own sources), t denotes the time period in years and V_{ocean} is the total volume of Hadean Ocean in liters. We have calculated a scenario for one million years using the present-day global ocean vol-

Table 7: Estimated increase in NH_4^+ concentration of the Hadean Ocean (in μmol.L^{-1}) from the hydrothermal N_2 reduction reaction per 1 Ma as a function of N_2-to-NH_4^+ conversion percentages, heat flow and percentage of heat released via hydrothermal systems.

5% of Earth's heat flow is released via hydrothermal activity					
N_2 conversion	*Hadean heat flow (× PDHF)*				
%	4	5	6	7	8
0.1	0.4	0.5	0.6	0.8	0.9
0.5	2.1	2.7	3.2	3.8	4.3
1	4.3	5.4	6.4	7.5	8.6
2	8.6	10.7	12.9	15.0	17.2
5	21.4	26.8	32.2	37.5	42.9
10	42.9	53.6	64.3	75.0	85.8
20% of Earth's heat flow is released via hydrothermal activity					
N_2 conversion	*Hadean heat flow (× PDHF)*				
%	4	5	6	7	8
0.1	1.7	2.1	2.6	3.0	3.4
0.5	8.6	10.7	12.9	15.0	17.2
1	17.2	21.4	25.7	30.0	34.3
2	34.3	42.9	51.5	60.0	68.6
5	85.8	107	129	150	172
10	172	214	257	300	343
80% of Earth's heat flow is released via hydrothermal activity					
N_2 conversion	*Hadean heat flow (× PDHF)*				
%	4	5	6	7	8
0.1	6.9	8.6	10.3	12.0	13.7
0.5	34.3	42.9	51.5	60.0	68.6
1	68.6	85.8	103	120	137
2	137	172	206	240	274
5	343	429	515	600	686
10	686	858	1030	1200	1370

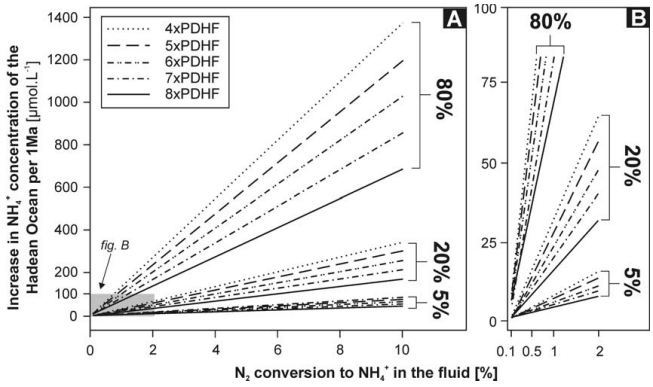

Figure 12
Estimated increase in NH_4^+ concentration of the Hadean Ocean (in μmol.L^{-1}) from the hydrothermal N_2 reduction reaction per 1 Ma as a function of N_2-to-NH_4^+ conversion percentages, heat flow and percentage of heat released via hydrothermal systems (5, 20 and 80%).

ume (1.37×10^{21} L) but alternative calculations can be quickly performed for different volumes (e.g., if the Hadean ocean had twice the volume of the present-day ocean, the NH_4^+ concentrations in Fig. 12 and Tab 7 would be 50% smaller). For example, the conversion of 0.5% of N_2 entrained in the advecting seawater would raise the NH_4^+ content of the (completely homogenized) Hadean ocean by ~8 to 17 μmol.kg^{-1} (4× to 8× PDHF) every 1 Ma (Tab. 7). These results (Fig. 12, Tab. 7) represent an upper contribution limit of this reaction, because no sinks (ion exchange, photooxidation, loss to the gas phase, formation of organic molecules, etc) were taken into account. In the absence of a comprehensive Hadean Nitrogen Cycle model, it is difficult to quantitatively assess the annual loss of NH_3/NH_4^+ from the ocean; however, the numbers in Fig. 12, Tab. 7 can be simply amended by assumption of loss expressed in %.

It is imperative to note that due to a large number of unknown and/or poorly constrained variables, these calculations should only be regarded as a first order approximation. However, it is clear that N2 reduction, albeit very inefficient, could have been a significant source of NH4+, especially in localized environments.

Because NO_2^-/NO_3^- are inherently easier to reduce than N_2, its presence in advected seawater could have significantly increased the annual NH_4^+ hydrothermal flux. It is unclear; however, how much NO_2^-/NO_3^- would be advected into the crust, especially in the presence of such significant sinks as the reduction by Fe(II) [5]. While this process is a viable pathway to abiotic NH_3/NH_4^+, its operation is dependent on atmospherically-driven processes of NO_2^-/NO_3^- formation as well as chemical composition of the Hadean Ocean, especially pH and mFe^{2+}. A change in one of the parameters (e.g., a shift in oceanic pH) may have negatively affected or completely halted this pathway. We assume that serpentinization-driven SHS would have been less affected by changes in ocean water chemistry because their physico-chemical conditions (e.g., pH, fH$_2$) are determined by fluid-rock interactions (e.g., availability of fresh rock) and possibly magmatic input rather than ocean composition. Moreover, the high temperature and pressure conditions combined with accumulations of suitable minerals would make these environments well suited for a long term, sustained NH_3/NH_4^+ production on the Hadean Earth.

Besides facilitating the production of NH_3/NH_4^+, metals and alloys in SHS may have been involved in other reac-

tions potentially important for prebiotic synthesis. In the context of environmental science, for example, Fe^0 was found to reduce nitrobenzene [91] or to facilitate reductive dehalogenation of carbon tetrachloride and chloroform [92-94]; Fe^{2+} sorbed on Fe(III) minerals decomposes nitrobenzene [60]. Our future research will also assess SHS as potential sinks of prebiotic molecules during the late Hadean/early Archaean.

The notion that N is commonly present in Fe^0 in its reduced form presents a possibility of meteoritic delivery of reduced N species to Earth, especially during the periods of heavy bombardment. Fe^0 and its alloys (e.g., tetrataenite, awaruite, kamacite) are among the dominant mineral phases in iron meteorites and to a lesser extent in stony-iron meteorites [e.g., [95]] [96-99].

To assess the possible importance of meteoric delivery of reduced N to Earth, we submitted four octahedrites for inert gas fusion analyses (IMR Test Labs, Lansing, NY). The meteorites – Bogou (IAB), Sikhote Alin (IIAB), Canyon Diablo (IAB), N'Goureyma (Ungrouped) [100-103] (Stony Brook University's meteorite collection) contained 22 to 32 ppm of N_{TOT} (Tab. 5). Although these analyses provided no insight into the oxidation state or speciation of nitrogen in these meteorites, it is likely to be present predominantly in the form of nitride (N^{3-}) as is the case in similar commercially available metals, alloys and known meteorite minerals (e.g., roaldite, carlsbergite). Hence in the following calculation we assume that all meteorite-associated nitrogen is present as nitride. Nitride would be readily released from meteorites after falling into the Hadean Ocean as a result of the rapid and complete dissolution due to inherent instability of Fe^0 in aqueous solutions (even in O_2-free solutions). Aqueous nitride is expected to react quickly with protons to form NH_3/NH_4^+. Similar scenario for meteoritic delivery of phosphorus has already been proposed by Pasek and collaborators [104,105].

To constrain the influx of meteoritic N to the Hadean Ocean we have adapted the meteorite flux values used by Pasek *et al* [104,105]: 2×10^5 kg.year^{-1} (current flux of iron meteorites to Earth; 50% of total meteoritic flux by weight) and meteoritic flux 10^5-10^6 times the present-day value during the Late Heavy Bombardment Period. Using these values we have created models for varying total reduced N content of iron meteorites: 5, 10, 15, 20, and 30 ppm. For comparison, average and median values for N_{TOT} from 91 published analyses [106,107] and four analyses acquired in this study were 20.1 and 12.3 ppm respectively.

The results presented in Fig. 13 show that during the Late Heavy Bombardment Period, iron meteorites could have

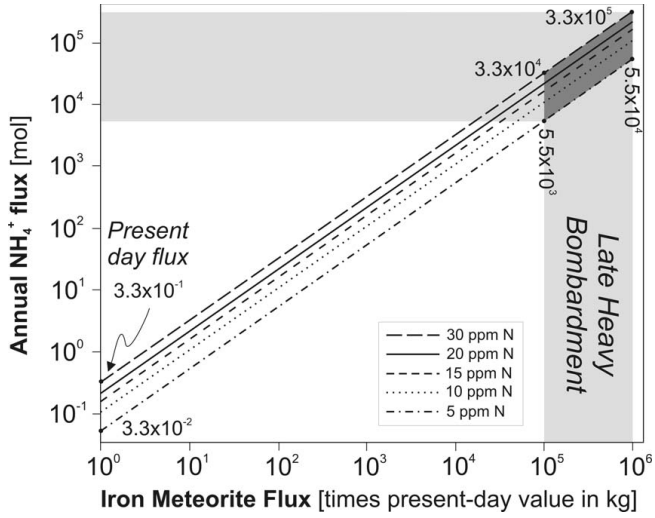

Figure 13
Estimated annual flux of nitrogen from iron meteorites. Different line styles correspond to different average N content of iron meteorites. Shaded areas represent iron meteorite flux during the period of Late Heavy Bombardment.

delivered ~10^3 to 10^5 mol.yr^{-1} of N_{TOT} to Earth which is approximately six to nine orders of magnitude less than our estimates for hydrothermal production (Fig. 11). Although the N influx was likely negligible on the global scale it is possible that crater lakes associated with iron meteorite impacts [108] may have contained significant concentrations of NH_3/NH_4^+. Environments containing NH_3/NH_4^+ and organic phosphorous compounds (e.g., phosphonates, organophosphates) from corroding iron meteorites ((Fe,Ni_3)P) [104,105] thus could have created very favorable, spatially-restricted conditions for prebiotic synthesis, perhaps unparalleled on the prebiotic Earth.

Conclusion

1) N_2 reduction to NH_4^+ was found to be limited (up to 2.5% at 200°C) compared to NO_2^-/NO_3^- (100% at 200°C)

2) Metals are more effective at reducing NO_2^-/NO_3^- than alloys; NH_4^+ is the dominant reaction product.

3) The reduction process exhibits a strong temperature dependence.

4) Fe^0 and Ni^0 were found to be least- and most resistant to alteration, respectively.

5) Ni^0, Fe^0, $Ni_{50}Fe_{50}$, $Ni_{81}Fe_{19}$ were found to contain up to 124 ppm of nitrogen in their structures, some of which is released upon dissolution and reacts to form NH_4^+.

6) Serpentinization-driven SHS were likely important sources of abiotic NH_3/NH_4^+ in the Hadean Ocean.

Competing interests

The authors declare that they have no competing interests.

Acknowledgements

This research was funded by NASA Exobiology Program (grant NAG 513438) to Martin Schoonen. Francis McCubbin is thanked for help with electron probe microanalysis. Matthew Wander's (SBU) comments and insight into mechanisms of N reduction are much appreciated. We are also thankful to Matthew Pasek (U. Arizona) for comments on N flux from iron meteorites. We appreciate the help of two anonymous reviewers for their valuable comments on an earlier version of this article. Dr. Ken B. Anderson is thanked for editorial handling of the manuscript.

References

1. Hennet RJC, Holm NG, Engel MH: **Abiotic synthesis of amino acids under hydrothermal conditions and the origin of life - A perpetual phenomenon.** *Naturwissenschaften* 1992, **79(8):**361-365.
2. Marshall WL: **Hydrothermal synthesis of amino acids.** *Geochim Cosmochim Ac* 1994, **58(9):**2099-2106.
3. Miller SL: **A production of amino acids under possible primitive Earth conditions.** *Science* 1953, **117(3046):**528-529.
4. Summers DP: **Sources and sinks for ammonia and nitrite on the early earth and the reaction of nitrite with ammonia.** *Orig Life Evol Biosph* 1999, **29(1):**33-46.
5. Summers DP, Chang S: **Prebiotic ammonia from reduction of nitrite by iron(II) on the early Earth.** *Nature* 1993, **365(6447):**630-632.
6. Summers DP: **Ammonia formation by the reduction of nitrite/nitrate by FeS: Ammonia formation under acidic conditions.** *Orig Life Evol Biosph* 2005, **35(4):**299-312.
7. Kasting JF: **Stability of ammonia in the primitive terrestrial atmosphere.** *J Geophys Res-Oc Atm* 1982, **87(NC4):**3091-3098.
8. Zahnle K: **Photochemistry of methane and the formation of Hydrocyanic Acid (HCN) in Earth's early atmosphere.** *J Geophys Res* 1986, **91(D2):**2819-2834.
9. Eugster HP, Munoz J: **Ammonium micas - Possible sources of atmospheric ammonia and nitrogen.** *Science* 1966, **151(3711):**683-686.
10. Schrauzer GN, Guth TD: **Photolysis of water and photoreduction of nitrogen on titanium dioxide.** *J Am Chem Soc* 1977, **99(22):**7189-7193.
11. Schrauzer GN, Strampach N, Hui LN, Palmer MR, Salehi J: **Nitrogen photo-reduction on desert sands under sterile conditions.** *P Natl Acad Sci USA* 1983, **80(12):**3873-3876.
12. Ranjit KT, Viswanathan B: **Photocatalytic reduction of nitrite and nitrate ions over doped TiO2 catalysts.** *J Photoch Photobio A* 1997, **107(1-3):**215-220.
13. Brandes JA, Boctor NZ, Cody GD, Cooper BA, Hazen RM, Yoder HS: **Abiotic nitrogen reduction on the early Earth.** *Nature* 1998, **395(6700):**365-367.
14. Schoonen MAA, Xu Y: **Nitrogen reduction under hydrothermal vent conditions: Implications for the prebiotic synthesis of C-H-O-N compounds.** *Astrobiology* 2001, **1(2):**133-141.
15. Dörr M, Kassbohrer J, Grunert R, Kreisel G, Brand WA, Werner RA, Geilmann H, Apfel C, Robl C, Weigand W: **A possible prebiotic formation of ammonia from dinitrogen on iron sulfide surfaces.** *Angew Chem Int Ed Engl* 2003, **42(13):**1540-1543.
16. Kelley DS, Fruh-Green GL: **Abiogenic methane in deep-seated mid-ocean ridge environments: Insights from stable isotope analyses.** *J Geophys Res-Planet* 1999, **104(B5):**10439-10460.
17. Mevel C: **Serpentinization of abyssal peridotites at mid-ocean ridges.** *CR Geosci* 2003, **335(10-11):**825-852.
18. Moody JB: **An experimental study on the serpentinization of iron-bearing olivines.** *Can Miner* 1976, **14:**462-478.
19. Filippidis A: **Chemical variation of olivine in the serpentinite of the central section in the Xerolivado chrome mine of Vourinos, Greece.** *Neues Jb Miner Abh* 1996, **170(2):**189-205.
20. Chamberlain JA, McLeod CR, Traill RJ, Lachance GR: **Native metals in the Muscox intrusion.** *Can J Earth Sci* 1965, **2:**189-215.
21. Dick HJB: **Terrestrial nickel-iron from Josephine peridotite, its geologic occurrence, associations, and origin.** *Earth Planet Sc Lett* 1974, **24:**291-298.
22. Ahmed Z, Bevan JC: **Awaruite, iridian awaruite, and a new Ru-Os-Ir-Ni-Fe alloy from the Sakhakot-Qila Complex, Malakand-Agency, Pakistan.** *Mineral Mag* 1981, **44(334):**225-230.
23. Eckstrand OR: **The Dumont serpentinite: A model for control of nickeliferous opaque mineral assemblages by alteration reactions in ultramafic rocks.** *Econ Geol* 1975, **70:**183-201.
24. Ashley PM: **Opaque mineral assemblage formed during serpentinization in the Coolac ultramafic belt, New South Wales.** *J Geol Soc Aust* 1975, **22:**91-102.
25. Alt JC, Shanks III WC: **Stable isotope compositions of serpentinite seamounts in the Mariana forearc: Serpentinization processes, fluid sources and sulfur metasomatism.** *Earth Planet Sc Lett* 2006, **242(3-4):**272-285.
26. Beard JS, Hopkinson L: **A fossil, serpentinization-related hydrothermal vent, Ocean Drilling Program Leg 173, Site 1068 (Iberia Abyssal Plain): Some aspects of mineral and fluid chemistry.** *J Geophys Res-Planet* 2000, **105(B7):**16527-16539.
27. Filippidis A: **Formation of awaruite in the system Ni-Fe-Mg-Si-O-H-S and olivine hydration with NaOH solution, an experimental study.** *Econ Geol* 1985, **80(7):**1974-1980.
28. Smirnov A: **Formation and Fate of Ammonium in the Hadean Ocean.** In *Department of Geosciences Volume PhD*. Stony Brook, NY , Stony Brook University; 2006:177.
29. Tian F, Toon OB, Pavlov AA, De Sterck H: **A hydrogen-rich early Earth atmosphere.** *Science* 2005, **308(5724):**1014-1017.
30. Kasting JF: **Earth's early atmosphere.** *Science* 1993, **259(5097):**920-926.
31. Navarro-Gonzalez R, McKay CP, Nna-Mvondo D: **A possible nitrogen crisis for Archaean life due to reduced nitrogen fixation by lightning.** *Nature* 2001, **412(6842):**61-64.
32. Nna-Mvondo D, Navarro G Rafael, Raulin F, Coll P: **Nitrogen fixation by corona discharge on the early Precambrian Earth.** *Origins Life Evol B* 2005, **35(5):**401-409.
33. Kasting JF: **Theoretical constraints on oxygen and carbon dioxide concentrations in the Precambrian atmosphere.** *Precambrian Res* 1987, **34(3-4):**205-229.
34. Mancinelli RL, McKay CP: **The evolution of nitrogen cycling.** *Origins Life Evol B* 1988, **18(4):**311-325.
35. ASTM-E-1019-00: **Standard test methods for determination of carbon, sulfur, nitrogen and oxygen in steel and in iron, nickel and cobalt alloys.** In *Annual Book of ASTM Standards Volume 03.05*. ASTM International; 2002:754-773.
36. Bethke CM: **The Geochemist's Workbench, Release 5.0.** University of Illinois; 2004.
37. Howald RA: **The thermodynamics of tetrataenite and awaruite: A review of the Fe-Ni phase diagram.** *Metall Mater Trans A* 2003, **34A(9):**1759-1769.
38. Davis JR: **Nickel, cobalt and their alloys.** Materials Park, OH , ASM International; 2000:442.
39. Kodentsov AA, van Dal MJH, Cserhati C, Daroczi L, van Loo FJJ: **Permeation of nitrogen in solid nickel and deformation phenomena accompanying internal nitridation.** *Acta Mater* 1999, **47(11):**3169-3180.
40. Cottrell AH: **An introduction to metallurgy.** London , Edward Arnold Publishers Ltd.; 1968:548.
41. Beddoes J, Parr JG: **Introduction to stainless steel.** 3rd edition. Materials Park, OH , ASM International; 1998:315.
42. Ech-chamikh E, Essafti A, Ijdiyaou Y, Azizan M: **XPS study of amorphous carbon nitride (a-C:N) thin films deposited by reactive RF sputtering.** *Solar Energy Materials and Solar Cells* 2006, **90(10):**1420-1423.
43. Jennings JR: **Catalytic ammonia synthesis.** New York , Plenum Press; 1991:476.
44. Ertl G: **Elementary steps in Ammonia synthesis: The surface science approach.** In *Catalytic ammonia synthesis* Edited by: Jennings JR. New York , Plenum Publishing; 1991:109-132.
45. Alberty RA: **Thermodynamics of the nitrogenase reactions.** *J Biol Chem* 1994, **269(10):**7099-7102.
46. Howard JB, Rees DC: **Structural basis of biological nitrogen fixation.** *Chem Rev* 1996, **96(7):**2965-2982.

47. Moody JB: **Serpentinization - Review.** *Lithos* 1976, **9(2):**125-138.
48. Reardon EJ: **Anaerobic corrosion of granular iron: Measurement and interpretation of hydrogen evolution rates.** *Environ Sci Technol* 1995, **29(12):**2936 -22945.
49. Chen YM, Li CW, Chen SS: **Fluidized zero valent iron bed reactor for nitrate removal.** *Chemosphere* 2005, **59(6):**753-759.
50. Cheng IF, Muftikian R, Fernando Q, Korte N: **Reduction of nitrate to ammonia by zero-valent iron.** *Chemosphere* 1997, **35(11):**2689-2695.
51. Choe SH, Ljestrand HM, Khim J: **Nitrate reduction by zero-valent iron under different pH regimes.** *Appl Geochem* 2004, **19(3):**335-342.
52. Hu HY, Goto N, Fujie K: **Effect of pH on the reduction of nitrite in water by metallic iron.** *Water Res* 2001, **35(11):**2789-2793.
53. Huang CP, Wang HW, Chiu PC: **Nitrate reduction by metallic iron.** *Water Res* 1998, **32(8):**2257-2264.
54. Huang YH, Zhang TC: **Effects of low pH on nitrate reduction by iron powder.** *Water Res* 2004, **38(11):**2631-2642.
55. Huang YH, Zhang TC: **Enhancement of nitrate reduction in Fe-0-packed columns by selected cations.** *J Environ Eng-ASCE* 2005, **131(4):**603-611.
56. Huang YH, Zhang TC, Shea PJ, Comfort SD: **Effects of oxide coating and selected cations on nitrate reduction by iron metal.** *J Environ Qual* 2003, **32(4):**1306-1315.
57. Alowitz MJ, Scherer MM: **Kinetics of nitrate, nitrite, and Cr(VI) reduction by iron metal.** *Environ Sci Technol* 2002, **36(3):**299-306.
58. Cruz-Carrera BME, Arancibia CG: **Influence of metallic cadmium on the electrochemical reduction of nitrate and nitrite ions.** *An Quim B-Inorg Anal* 1980, **76(2):**267-272.
59. Wärna J, Turunen I, Salmi T, Maunula T: **Kinetics of nitrate reduction in monolith reactor.** *Chem Eng Sci* 1994, **49(24B):**5763-5773.
60. Klausen J, Tröber SP, Haderlein SB, Schwarzenbach RP: **Reduction of substituted nitrobenzenes by Fe(II) in aqueous mineral suspensions.** *Environ Sci Technol* 1995, **29:**2396-2404.
61. Weber EJ: **Iron-mediated reductive transformations: Investigation of reaction mechanism.** *Environ Sci Technol* 1996, **30(2):**716 -7719.
62. Huang YH, Zhang TC: **Effects of dissolved oxygen on formation of corrosion products and concomitant oxygen and nitrate reduction in zero-valent iron systems with or without aqueous Fe2+.** *Water Res* 2005, **39(9):**1751-1760.
63. Sorensen J, Thorling L: **Stimulation by Lepidocrocite (gamma-FeOOH) of Fe(II)-dependent nitrite reduction.** *Geochim Cosmochim Ac* 1991, **55(5):**1289-1294.
64. Seo M, Sato N: **Selective surface oxidation of Fe30-Ni alloy: Mt. Fuji, Lake Yamanaka, Japan.** The Japan Institute of Metals; 1982:175-182.
65. Neely JE, Bertone TJ: **Practical metallurgy and materials of industry.** 6th edition. Upper Saddle River, NJ , Prentice Hall; 2002:464.
66. Cooley WE: **Nickel.** In *McGraw-Hill encyclopedia of chemistry* Edited by: Parker SP. New York , McGraw-Hill, Inc.; 1993.
67. Epron F, Gauthard F, Pineda C, Barbier J: **Catalytic reduction of nitrate and nitrite on Pt-Cu/Al2O3 catalysts in aqueous solution: Role of the interaction between copper and platinum in the reaction.** *J Catal* 2001, **198(2):**309-318.
68. Gauthard F, Epron F, Barbier J: **Palladium and platinum-based catalysts in the catalytic reduction of nitrate in water: effect of copper, silver, or gold addition.** *J Catal* 2003, **220(1):**182-191.
69. Hoashi M, Brooks RR, Reeves RD: **Palladium, platinum and rhutenium in iron meteorites and their taxonomic significance.** *Chem Geol* 1993, **106:**207-218.
70. Tolstykh N, Krivenko A, Sidorov E, Laajoki K, Podlipsky M: **Ore mineralogy of PGM placers in Siberia and the Russian Far East.** *Ore Geol Rev* 2002, **20(1-2):**1-25.
71. Cawthorn RG, Lee CA, Schouwstra RP, Mellowship P: **Relationship between PGE and PGM in the Bushveld Complex.** *Can Miner* 2002, **40:**311-328.
72. Schoonen MAA, Smirnov A, Cohn C: **A perspective on the role of minerals in prebiotic synthesis.** *Ambio* 2004, **33(8):**539-551.
73. Blesa MA, Matijevič E: **Phase transformations of iron oxides, oxohydroxides, and hydrous oxides in aqueous media.** *Adv Colloid Interfac Sci* 1989, **29(3-4):**173-221.
74. Refait P, Memet JB, Bon C, Sabot R, Genin JMR: **Formation of the Fe(II)-Fe(III) hydroxysulphate green rust during marine corrosion of steel.** *Corros Sci* 2003, **45(4):**833-845.
75. Cornell RM, Schwertmann U: **The Iron Oxides: Structure, Properties, Reactions, Occurrences and Uses.** 2nd edition. Weinheim , Wiley; 2003:703.
76. Hansen HCB, Koch CB, NanckeKrogh H, Borggaard OK, Sorensen J: **Abiotic nitrate reduction to ammonium: Key role of green rust.** *Environ Sci Technol* 1996, **30(6):**2053-2056.
77. Hansen HCB, Koch CB: **Reduction of nitrate to ammonium by sulphate green rust: activation energy and reaction mechanism.** *Clay Miner* 1998, **33(1):**87-101.
78. Rakshit S, Matocha CJ, Haszler GR: **Nitrate reduction in the presence of wustite.** *J Environ Qual* 2005, **34(4):**1286-1292.
79. Ottley CJ, Davison W, Edmunds WM: **Chemical catalysis of nitrate reduction by iron (II).** *Geochim Cosmochim Ac* 1997, **61(9):**1819-1828.
80. Wander MCF, Kubicki JD, Schoonen MAA: **Reduction of N2 by Fe2+ - comparison of homogeneous and heterogeneous reactions: A theoretical study.** In *Astrobiology Volume 6*. Issue 1 Washington, DC ; 2006:112.
81. Abbott DH, Hoffman SE: **Archaean plate tectonics revisited. 1. Heat flow, spreading rate, and the age of subducting oceanic lithosphere and their effects on the origin and evolution of continents.** *Tectonics* 1984, **3(4):**429-448.
82. Turcotte DL: **On the thermal evolution of the Earth.** *Earth Planet Sc Lett* 1980, **48:**53-58.
83. Elderfield H, Schultz A: **Mid-ocean ridge hydrothermal fluxes and the chemical composition of the ocean.** *Annu Rev Earth Pl Sc* 1996, **24:**191-224.
84. Kasting JF: **Bolide impacts and the oxidation state of carbon in the Earth's early atmosphere.** *Origins Life Evol B* 1990, **20(3-4):**199-231.
85. Charlou JL, Fouquet Y, Bougault H, Donval JP, Etoubleau J, Jean-Baptiste P, Dapoigny A, Appriou P, Rona PA: **Intense CH4 plumes generated by serpentinization of ultramafic rocks at the intersection of the 15 degrees 20 ' N fracture zone and the Mid-Atlantic Ridge.** *Geochim Cosmochim Ac* 1998, **62(13):**2323-2333.
86. Kelley DS, Karson JA, Blackman DK, Fruh-Green GL, Butterfield DA, Lilley MD, Olson EJ, Schrenk MO, Roe KK, Lebon GT, Rivizzigno P: **An off-axis hydrothermal vent field near the Mid-Atlantic Ridge at 30 degrees N.** *Nature* 2001, **412(6843):**145-149.
87. Von Damm KL: **Seafloor hydrothermal activity - Black smoker chemistry and chimneys.** *Annu Rev Earth Pl Sc* 1990, **18:**173-204.
88. Macleod G, McKeown C, Hall AJ, Russell MJ: **Hydrothermal and oceanic pH conditions of possible relevance to the origin of life.** *Orig Life Evol Biosph* 1994, **24(1):**19-41.
89. Bischoff JL, Rosenbauer RJ: **An empirical equation of state for hydrothermal seawater (3.2 percent NaCl).** *Am J Sci* 1985, **285:**725-763.
90. Gaventman LH: **Solubility of selected gases in water.** In *CRC Handbook of Chemistry and Physics* 75th edition. Edited by: Lide DR. Boca Raton , CRC Press; 1994:6-3.
91. Agrawal A, Tratnyek PG: **Reduction of nitroaromatic compounds by zero-valent iron metal.** *Environ Sci Technol* 1996, **30:**153-150.
92. Matheson LJ, Tratnyek PG: **Reductive dehalogenation of chlorinated methanes by iron metal.** *Environ Sci Technol* 1994, **28:**2045-2053.
93. Warren KD, Arnold RG, Bishop TL, Lindholm LC, Batterton EA: **Kinetics and mechanism of reductive dehalogenation of carbon tetrachloride using zero-valent metals.** *J Hazard Mater* 1995, **41:**217-227.
94. Gillham RW, O'Hannesin F: **Enhanced degradation of halogenated aliphatics by zero-valent iron.** *Ground Water* 1994, **32(6):**958-967.
95. D'Orazio M, Folco L, Perchiazzi N: **The Bagnone iron meteorite (Tuscany, Italy): History, mineralogy, and chemical classification.** *Meteorit Planet Sci* 2004, **39(8):**A133-A138.
96. Rubin AE: **Euhedral awaruite in the Allende meteorite: Implications for the origin of awaruite- and magnetite-bearing nodules in CV3 chondrites.** *Am Mineral* 1991, **76(1356-1362):**.
97. Nagata T, Carleton BJ: **Tetrataenite in carbonaceous chondrites.** *P Jpn Acad B-Phys* 1990, **66(10):**183-188.

98. Nagata T, Carleton BJ: **Tetrataenite in chondritic meteorites.** *P Jpn Acad B-Phys* 1989, **65(6):**121-124.
99. Gattacceca J, Rochette P, Bourot-Denise M: **Magnetic properties of a freshly fallen LL ordinary chondrite: the Bensour meteorite.** *Phys Earth Planet In* 2003, **140(4):**343-358.
100. Foote AE: **Meteoritic iron of Canyon Diablo.** *Am J Sci* 1891, **42:**413-417.
101. Unik JP, Henderson DJ, Huizenga JR: **Radioactive species produced by cosmic rays in the Bogou iron meteorite.** *Geochim Cosmochim Ac* 1964, **28:**593-594.
102. Yavnel AA: **Issledovanie struktury Sikhote-Alinskogo meteorita.** *Dokl Akad Nauk* 1948, **60(8):**1381-1384.
103. Cohen E: **Meteoric iron from N'Goureyma, near Djenne, Province of Macina, Soudan.** *Am J Sci* 1903, **15(88):**254-258.
104. Pasek M, Lauretta DS: **Aqueous corrosion of phosphide minerals from iron meteorites: A highly reactive source of prebiotic phosphorus on the surface of the early Earth.** *Astrobiology* 2005, **5(4):**515-535.
105. Pasek MA, Dworkin JP, Lauretta DS: **A radical pathway for organic phosphorylation during schreibersite corrosion with implications for the origin of life.** *Geochim Cosmochim Ac* 2007, **71(7):**1721-1736.
106. Franchi IA, Wright IP, Pillinger CT: **Constraints on the formation conditions of iron meteorites based on concentrations and isotopic compositions of iron meteorites.** *Geochim Cosmochim Ac* 1993, **57:**3105-3121.
107. Prombo CA, Calyton RN: **Nitrogen isotopic compositions of iron meteorites.** *Geochim Cosmochim Ac* 1993, **57:**3749-3761.
108. Bland PA, Artemieva NA: **The rate of small impacts on Earth.** *Meteorit Planet Sci* 2006, **41:**607-631.
109. Peretti A, Dubessy J, Mullis J, Frost BR, Trommsdorff V: **Highly reducing conditions during Alpine metamorphism of the Malenco peridotite (Sondrio, Northern Italy) indicated by mineral paragenesis and H2 in fluid inclusions.** *Contrib Mineral Petr* 1992, **112(2-3):**329-340.
110. Tarkian M, Economou-Eliopoulos M, Sambanis G: **Platinum-group minerals in chromitites from the Pindos ophiolite complex, Greece.** *Neues Jahrbuch Fur Mineralogie-Monatshefte* 1996, **4:**145-160.
111. Auge T, Cabri LJ, Legendre O, McMahon G, Cocherie A: **PGE distribution in base-metal alloys and sulfides of the New Caledonia ophiolite.** *Can Miner* 1999, **37:**1147-1161.
112. Agafonov LV, Lesnov FP: **Platinoids in websterites from the Narun Massif of mafic and ultramafic rocks (Western Mongolia).** *Geol Geofiz* 1997, **38(12):**1949-1954.
113. Arai S, Prichard HM, Matsumoto I, Fisher PC: **Platinum-group minerals in podiform chromitite from the Kamuikotan zone, Hokkaido, northern Japan.** *Resour Geol* 1999, **49(1):**39-47.
114. Zhmodik SM, Agafonov LV: **Shandite and other nickel minerals from chromitites of ophiolite association in the southeast of East Sayan.** *Geol Geofiz* 2000, **41(5):**712-721.
115. Ahmed Z: **Comparison of the geochemistry of ophiolitic pyroxenites with a strongly fractionated dyke of pyroxenite from the Sakhakot-Qila Ophiolite, Pakistan.** *Chem Geol* 1991, **91(4):**335-355.